

Field Patterns: A New Mathematical Object

Graeme W. Milton and Ornella Mattei

Department of Mathematics, University of Utah, Salt Lake City UT 84112, USA

Abstract

Field patterns occur in space-time microstructures such that a disturbance propagating along a characteristic line, does not evolve into a cascade of disturbances, but rather concentrates on a pattern of characteristic lines. This pattern is the field pattern. In one spatial direction plus time, the field patterns occur when the slope of the characteristics is, in a sense, commensurate with the space-time microstructure. Field patterns with different spatial shifts do not generally interact, but rather evolve as if they live in separate dimensions, as many dimensions as the number of field patterns. Alternatively one can view a collection as a multicomponent potential, with as many components as the number of field patterns. Presumably if one added a tiny nonlinear term to the wave equation one would then see interactions between these field patterns in the multidimensional space that one can consider them to live, or between the different field components of the multicomponent potential if one views them that way. As a result of \mathcal{PT} -symmetry many of the complex eigenvalues of an appropriately defined transfer matrix have unit norm and hence the corresponding eigenvectors correspond to propagating modes. There are also modes that blow up exponentially with time.

1 Introduction

Here we introduce the theory of field patterns. Field patterns develop when waves, concentrated on characteristic lines, interact with certain special space-time microstructures. They occur when the space-time microstructure is such that the propagation along characteristics does not develop into a complicated cascade of space-time lines, but rather concentrates along particular patterns: these are the field patterns. There is an obvious connection with dynamical systems.

What makes field patterns mathematically novel is their appearance in wave equations and the associated multidimensional, or multicomponent, character of a collection of field patterns even though the wave equation is, say, a scalar wave-equation in 1-, 2-, or 3-dimensions plus time. Here for simplicity we will focus on the appearance of field patterns in scalar wave equations in 1 spatial dimension plus time.

The field patterns we introduce here can have both a particle-like aspect, as the patterns are concentrated on lines in space-time, and a wave-like aspect, as the patterns at long times can develop wave-like features. This hints of a connection with quantum mechanics. Another connection is the multidimensional nature of field patterns. In the noninteracting model of field patterns developed here, different field patterns in a collection, while occupying the same space-time continuum, act as if they live in separate dimensions. The multidimensional nature of collections of field patterns is quite different to that associated with multiscale homogenization theory. In multiscale homogenization, with say periodicity at all but the largest length scale, the moduli of the materials and the fields are often modeled in d -dimensions by functions of the form

$$u_\epsilon(\mathbf{x}) = f(\mathbf{x}, \mathbf{x}/\epsilon, \mathbf{x}/\epsilon^2, \mathbf{x}/\epsilon^3, \dots, \mathbf{x}/\epsilon^{m-1}), \quad (1.1)$$

where $\epsilon > 0$ is a very small parameter giving the ratio between length scales and $f(\mathbf{x}, \mathbf{y}_1, \mathbf{y}_2, \mathbf{y}_3, \dots, \mathbf{y}_{m-1})$ is a function living in a md dimensional space, that is periodic in each of the variables $\mathbf{y}_1, \mathbf{y}_2, \dots, \mathbf{y}_m$, but not necessarily periodic in \mathbf{x} (see, for example, [1, 2, 3, 4]). Conversely, the notions of two-scale and multiscale convergence [5, 6] allow one to go from sequences of functions $u_\epsilon(\mathbf{x})$ parametrized by ϵ to the multidimensional function $f(\mathbf{x}, \mathbf{y}_1, \mathbf{y}_2, \mathbf{y}_3, \dots, \mathbf{y}_{m-1})$. In this multiscale homogenization, the different dimensions $\mathbf{x}, \mathbf{y}_1, \mathbf{y}_2, \mathbf{y}_3, \dots, \mathbf{y}_{m-1}$ play very different roles, each associated with a different length scale. By contrast, the different dimensions associated with a collection of field

patterns play more or less an equivalent role, as do the different dimensions associated with say the multielectron Schrödinger equation. Rather than using a multidimensional space, an alternative way of viewing noninteracting field patterns is as a multicomponent potential, where each component potential is associated with one field pattern.

We do not study models where there are interactions between the field patterns. This would require adding non-linear terms to the wave equation. Without such terms, a superposition of two field pattern solutions is also a solution: the field patterns do not interact.

Some quantum mechanical aspects are notably absent from the models we study here: significantly, there is nothing analogous to the collapse of the wave-function; there is no stochastic element in the evolutions we describe here; and moreover there is no quantization of the solutions. It is curious that some of these quantum mechanical aspects have been seen in the dynamics of "walking droplets" of silicon oil on a vibrating silicon oil fluid surface, that may be interpreted as a space-time microstructure [7, 8, 9]. In a certain region of instability, these droplets start "walking", creating their own "pilot wave" on the surface. The trajectory of the droplet can seem stochastic as the motion of a droplet after a bounce depends on the orientation of the fluid surface where it lands, and this can appear quite random: nevertheless the ensemble averaged statistics exhibit wave-like features. The "holy-grail" would be that a complete explanation of quantum mechanics emerges from a combination of these "pilot wave" ideas, and the ideas in the theory of field patterns introduced here. The bold conjecture is that the fundamental objects in the universe are neither particles, nor waves, but field patterns. In this regard, it seems likely that the associated space-time microstructure would have a length scale comparable to the Planck length (about 10^{-35} meters) and a time scale comparable to the Planck time (about 10^{-44} seconds).

Space-time microstructures are composites whose microstructure varies not just with respect to space but also with respect to time. There exist two natural ways of changing the material properties in time, thus, leading to two types of space-time microstructure. Using the terminology in the book of Lurie [10] *activated materials* (the subject matter of this article) are immovable with respect to the laboratory frame and the space-time microstructure is realized by an external mechanism that produces a time switching (either instantaneous or gradual) of the space pattern of the material in a pre-determined manner; in *kinetic materials*, instead, the space-time microstructure is realized by an actual mechanical motion of the various parts of the composite system with respect to the laboratory frame. In other words, in activated materials the motion (without transfer of matter) is only in terms of the property pattern, whereas in kinetic materials the space-time microstructure is achieved by moving fragments of the material assemblage. Clearly, standard composites can be considered as space-time microstructures with a microstructure that depends only on space. Activated materials are most easily achieved (see, for example, [11]) by propagating a large amplitude wave (the "pump wave") into a non-linear homogeneous, or possibly inhomogeneous, medium. One could even propagate several large amplitude waves that then form an interference pattern. On top of these large waves one superimposes waves that are sufficiently small that one can linearize the problem and treat them as if they are propagating in a medium with space-time variations given by the tangent moduli associated with the large amplitude waves. There are many other ways of creating space-time geometries too. For instance, one could consider a spatially periodic two-phase geometry where one phase is a liquid crystal and then subject this material to an oscillating electric field that then causes a temporal modulation in the refractive index of the liquid crystal phase.

Space-time microstructures were studied as early as 1958 by Cullen [12], who noted that a transmission line, with modulated inductance that propagates along the line, could support a current wave that is periodic in time but grows exponentially along the transmission line (in space). This transmission line, with time varying modulated inductance, can be viewed as a "space-time laminate with continuously varying moduli" in which the moduli are just functions of $\mathbf{n} \cdot \mathbf{x}$, where \mathbf{x} and \mathbf{n} are two-dimensional vectors and we identify the components of \mathbf{x} , x_1 with space and x_2 with time. If one interchanges the roles of time and space (switching x_1 and x_2) in the analysis of Cullen, one naturally gets a "space-time laminate" which supports a field that is exponentially growing in time. Shortly afterwards, space-time laminates that interact with a field $\mathbf{u} = (V_1, V_2)$ consisting of a pair of potentials V_1 and V_2 were investigated by Tien [13] who found that they could transfer power between waves at different frequencies. Morgenthaler [14], while studying electromagnetic wave propagation in a homogeneous dielectric medium with time-dependent permittivity and permeability, derived a solution for the cases of a two-layered temporal laminate and for a temporal graded material. Subsequently, Fante [15] proposed an explicit solution for the electromagnetic problem of a multi-layered temporal laminate with layers having the same wave impedance, and a solution in closed form for the case of layers with different wave impedances. Many more early references and an experimental validation can be found in the paper of Honey and Jones [16].

Activated space-time laminates (where the moduli only depend on $\mathbf{n} \cdot \mathbf{x}$ in which x_{d+1} is identified with time, and d is the number of spatial dimensions) are of particular interest as they exhibit remarkable properties: indeed,

by suitably controlling the design parameters it is possible to selectively screen large space-time domains from long wave disturbances [17, 18], an effect that is impossible to realize with standard laminates. In particular, waves cannot travel in the forward direction when the microstructure is effectively moving faster than the speed of wave propagation in an equivalent stationary medium. Contrary to what happens in other space-time microstructures, the total energy of two-component space-time laminates is preserved for low frequency waves: the energy pumped into the system to switch from one material to the other (say, from material 1 to material 2) is equal to the energy released at the subsequent switch (from material 2 to material 1) [19]. For such low frequency waves one can replace the laminated microstructure with a homogeneous one with suitable effective properties. The determination of these effective properties [17, 20, 21] follows the standard procedure for static laminates (see, for example, Chapter 9 of [22] and references therein) for which the homogenized parameters are easily derived through direct calculation. When the frequency is not low, one can regard the laminated structure as a spatially periodic structure, independent of time, that is rotated in space-time. Thus one can apply standard Bloch-Floquet theory, with a harmonic dependence on time replaced with a harmonic dependence on $\mathbf{m} \cdot \mathbf{x}$ where \mathbf{m} is perpendicular to \mathbf{n} . An additional assumption, which permits a lot of explicit analysis, is to assume that the fluctuations in the moduli are sinusoidal, only involving one Fourier component. Then the constitutive relation only couples together neighboring Fourier modes, and is easily solved [23, 24, 25]. For high frequency waves the energy balance need not occur, and waves can grow exponentially in time [26].

Besides space-time laminates, other space-time microstructures have been proposed in the literature. In particular, special attention has been drawn towards rectangular microstructures in one spatial dimension and time (e.g., [27] and [28]): the geometry is doubly-periodic in time and space, and the space period is of the same order of the time period. Specifically, the case of checkerboard geometries where the two constituent materials have the same wave impedance, so that there is not a reflected wave but only a transmitted wave, has been extensively investigated (e.g., [27]). Very interestingly, within each space period, the disturbances converge towards a so-called “limit cycle” after a few time periods, if the parameters of the constituents are suitably chosen. As a group of characteristics converges to a limit cycle, the energy of the macroscopic system grows exponentially (see, e.g., [29]). It is almost like shocks are developing in a linear medium. (One wonders if a stochastic version of such linear shocks could be a mechanism for the collapse of the wave function in quantum mechanics. Note that at the Planck length scale it is questionable as to whether the concept of energy has any meaning). In particular, the spatial derivative of the disturbance increases every time the wave passes through a pure spatial interface, whereas its time derivative grows every time the wave passes through a pure time interface [27]. Therefore, unlike space-time laminates at low frequencies, space-time checkerboard geometries accumulate energy independently of the frequency, and, clearly, this does not allow one to apply the standard homogenization techniques to determine the effective properties of the material. Nevertheless, the macroscopic behavior of such exponentially growing fields is probably described by some coarse grained equations. (We also find exponentially growing fields, yet it seems likely that macroscopic features, such as the conical shape seen later in Figure 13, might be describable by some coarse grained equations.) It is worth noting that another consequence of the exponentially accumulation of energy in macroscopic systems is the thermodynamic non-equilibrium of such materials which, on the contrary, seem to be thermodynamically open systems: only when analyzed together with the surrounding environment can they be considered as thermodynamically closed systems. We should point out that the crossing of pure temporal interfaces, in correspondence to which the properties of the material change instantaneously, leads to very interesting phenomena, such as the Doppler effect analyzed, for instance, by Rousseau et al. [30].

The extension of the theory to space-time microstructures with properties varying in a two-dimensional space and in time reveals new aspects totally absent in the one-dimensional case. For instance, in the work of Sanguinet [31], the homogenization of an elastic laminate in plane strain (with both inertial and elastic properties varying in time and space) leads to two new additional forces, one of which is of the Coriolis-type. This force, arising from the dynamics and the plane strain hypothesis, vanishes when the model is restricted to the one-dimensional case.

On the other hand, specific unconventional space-time microstructures have been designed to optimize certain properties by means of topology optimization. Following the pioneering papers of Maestre et al. [32] and Maestre and Pedregal [33], where the optimization of the distributions of materials in one-dimensional and two-dimensional space and in time has been studied, Jensen [34] proposed an optimized dynamic structure with time varying stiffness that prohibits wave propagation: it consists of a moving bandgap with layers of stiff inclusions moving with the propagating wave. These results have been also extended to the case of time varying mass density [35].

As space-time microstructures can break time reversal invariance, nonreciprocal frequency conversion [36, 37] and other nonreciprocal effects (see [38] and references therein) can occur. Moreover, most remarkably, Fang, Yu,

and Shan [39] show that one can get effective magnetic fields for photons by dynamic modulation. Also Yuan, Shi, and Fan [40], following related ideas of Boada, Celi, Latorre and Lewenstein [41] and Celi, Massignan, Ruseckas, Goldman, Spielman, Juzeliūnas and M. Lewenstein [42], find that it is useful to introduce an extra "synthetic frequency" dimension in the modeling of the behavior of arrays of resonators undergoing a time-harmonic refractive index modulation, and this has lead to interesting ideas such as optical models of four-dimensional quantum Hall physics [43] and simulated Weyl points [44].

Irrespective of the fascinating possible connection of the theory of field patterns to quantum mechanics, the theory of field patterns is intrinsically interesting and could prove relevant in the study of spatially periodic composites of hyperbolic materials. Hyperbolic materials are materials where the dielectric tensor has both positive and negative eigenvalues. They were studied in the context of anisotropic plasmas by Fisher and Gould [45] back in 1969, albeit with an antisymmetric part added to the dielectric tensor. In any physical hyperbolic material these eigenvalues also have a small imaginary part that causes absorption of electromagnetic energy into heat. The simplest way to obtain hyperbolic materials is simply to laminate an isotropic material with positive dielectric constant with a material with negative dielectric constant at the frequency under consideration: candidates for materials with negative dielectric constant over a frequency range include silver, gold, and silicon carbide as well as host of novel materials [46]. If one assumes that homogenization theory applies (and the conditions for this assumption to be valid warrant further investigation), then the effective dielectric constant of the laminate is given by the arithmetic average in any direction parallel to the layers, and by the harmonic mean in the direction orthogonal to the layers. The key point is that the harmonic averages and arithmetic averages are sometimes of opposite sign, giving rise to a hyperbolic effective dielectric tensor. There are also naturally occurring hyperbolic materials [47]. Hyperbolic materials have generated considerable interest as they can direct radiation along the "characteristic lines" in the hyperbolic medium. With the hyperbolic medium in a shell configuration, and the material oriented so an eigenvector of the dielectric tensor points in the radial direction, sources near the inner boundary of the shell can be spaced less than a wavelength apart, yet radiate along the characteristic lines to the outer surface of the shell where they can be greater than half a wavelength apart and thus detectable through conventional microscopic techniques. Thus this "hyperlens", proposed by Jacob, Alekseyev, and Narimanov [48] and by Salandrino and Engheta [49], that was subsequently experimentally validated [50, 51], allows one to resolve sources that are less than a wavelength apart. In the quasistatic regime, where the wavelength is much larger than the body under consideration, the governing equations are

$$\mathbf{d}(\mathbf{x}) = \boldsymbol{\varepsilon}(\mathbf{x})\mathbf{e}(\mathbf{x}), \quad \text{where} \quad \nabla \cdot \mathbf{d} = 0, \quad \mathbf{e} = -\nabla V, \quad (1.2)$$

where $\mathbf{d}(\mathbf{x})$, the electric displacement field, $\mathbf{e}(\mathbf{x})$, the electric field, $V(\mathbf{x})$, the electric potential, and $\boldsymbol{\varepsilon}(\mathbf{x})$ the dielectric tensor, are all complex valued. Consider the simplest case where the material and fields are two-dimensional (or three-dimensional but independent of one spatial coordinate), and the dielectric tensor is diagonal and hyperbolic,

$$\boldsymbol{\varepsilon}(\mathbf{x}) = \begin{pmatrix} \alpha(\mathbf{x}) & 0 \\ 0 & -\beta(\mathbf{x}) \end{pmatrix}, \quad (1.3)$$

in which $\alpha(\mathbf{x})$ and $-\beta(\mathbf{x})$ are complex valued functions with non-negative imaginary part. Then (1.2) reduces to

$$\frac{\partial}{\partial x_1} \left[\alpha(\mathbf{x}) \frac{\partial V}{\partial x_1} \right] = \frac{\partial}{\partial x_2} \left[\beta(\mathbf{x}) \frac{\partial V}{\partial x_2} \right]. \quad (1.4)$$

In regions where $\alpha(\mathbf{x})$ and $\beta(\mathbf{x})$ are constant, real, and positive this is just the standard wave equation if one reinterprets x_2 as a time coordinate, keeping x_1 as a spatial coordinate. So a spatially periodic hyperbolic material where the dielectric tensor takes the form (1.3) can be viewed in the limit where the loss goes to zero as a space-time microstructure. An interesting question is whether in spatially periodic composites of hyperbolic materials one can get unusual homogenized equations in the limit where the imaginary part of $\alpha(\mathbf{x})$ and $\beta(\mathbf{x})$ tends to zero. One might expect that such unusual homogenized behavior could occur if the "cell-problem", where one looks for periodic $\mathbf{d}(\mathbf{x})$ and $\mathbf{e}(\mathbf{x})$ that solve (1.2) with a prescribed non-zero average value of $\mathbf{e}(\mathbf{x})$, has a nonunique solution when the loss is zero.

We should point out that besides the study of space-time microstructures, there is a large body of work on active control by using structures with moduli that vary in space and time (see, for instance, [52], [53], and [54]). Also, interestingly, space-time boundaries have been found to be important for time reversal [55, 56]: a wave pulse hitting a space-time boundary divides into two wave pulses: one continues to spread outwards and the other converges to

the position of the original source. This division of wave pulses is also apparent in the work of Lurie and coworkers [17, 18, 57, 28].

Subsequent to the initial phases of this work it was discovered by Alexander and Natalia Movchan that field patterns occur in space-time geometries that are as simple as a two-phase laminate with boundaries that are normal to the time axis (i.e, at a periodic set of times). The analysis of this will be explored elsewhere [58].

2 Statement of the problem

To begin with, and to keep things simple, our first interest is in the two-dimensional conductivity equation

$$\mathbf{j}(\mathbf{x}) = \boldsymbol{\sigma}(\mathbf{x})\mathbf{e}(\mathbf{x}), \quad \text{where} \quad \nabla \cdot \mathbf{j} = 0, \quad \mathbf{e} = -\nabla V, \quad (2.1)$$

with $\mathbf{j}(\mathbf{x})$ the electric current, $\mathbf{e}(\mathbf{x})$ the electric field, $V(\mathbf{x})$ the electric potential, and $\boldsymbol{\sigma}(\mathbf{x})$ the conductivity tensor. Here we focus only on the conductivity problem of an assemblage of two materials, that is, we study the case where $\boldsymbol{\sigma}(\mathbf{x})$ can take only two values:

$$\boldsymbol{\sigma}(\mathbf{x}) = \chi(\mathbf{x})\boldsymbol{\sigma}_1 + [1 - \chi(\mathbf{x})]\boldsymbol{\sigma}_2, \quad (2.2)$$

where $\chi(\mathbf{x})$ is a characteristic function that takes the value 1 in the region of the material where $\boldsymbol{\sigma}(\mathbf{x}) = \boldsymbol{\sigma}_1$ and takes the value 0 in the region where $\boldsymbol{\sigma}(\mathbf{x}) = \boldsymbol{\sigma}_2$, with the conductivities $\boldsymbol{\sigma}_1$ and $\boldsymbol{\sigma}_2$ taking the form

$$\boldsymbol{\sigma}_1 = \begin{pmatrix} \alpha_1 & 0 \\ 0 & -\beta_1 \end{pmatrix}, \quad \boldsymbol{\sigma}_2 = \begin{pmatrix} \alpha_2 & 0 \\ 0 & -\beta_2 \end{pmatrix}, \quad (2.3)$$

where the parameters α_i and β_i , $i = 1, 2$ are, in general, real and positive. The reason why the conductivity coefficient in the x_2 direction is taken to be negative is merely for the sake of convenience. In fact, in such a way, it is easy to see that by combining equations (2.1) and (2.3), the potential $V_i(\mathbf{x})$ in phase i , $i = 1, 2$, satisfies the following wave equation

$$\alpha_i \frac{\partial^2 V_i}{\partial x_1^2} = \beta_i \frac{\partial^2 V_i}{\partial x_2^2}. \quad (2.4)$$

Indeed, we can think of x_1 representing the space variable x , and x_2 as representing the time variable t . Consequently, the parameters α_i , $i = 1, 2$, are nothing but the usual conductivity coefficients in space, whereas the β_i , $i = 1, 2$, have to be interpreted as the conductivity coefficients in time. In other words, we are considering a one-dimensional distribution of the two materials and we suppose that such a configuration varies not just with respect to the spatial coordinate x but also with respect to time, thus giving rise to a dynamic material.

It is well-known that the local solution in phase i of equation (2.4), deduced via d'Alembert method, is simply given by

$$V_i(x, t) = V_i^+(x - c_i t) + V_i^-(x + c_i t) \quad (2.5)$$

where $V_i^+(x - c_i t)$ is the wave moving upwards to the right in a space-time diagram, $V_i^-(x + c_i t)$ is the wave moving upwards to the left in a space-time diagram, and

$$c_i = \sqrt{\alpha_i / \beta_i} \quad (2.6)$$

is the wave space. Note that associated with $V_i^+(x - c_i t)$ and $V_i^-(x + c_i t)$ are currents

$$\begin{aligned} \mathbf{j}_i^+ &= -\boldsymbol{\sigma}_i \nabla V_i^+(x - c_i t) = \sqrt{\alpha_i \beta_i} \begin{pmatrix} -c_i \\ -1 \end{pmatrix} V_i^{+'}(x - c_i t), \\ \mathbf{j}_i^- &= -\boldsymbol{\sigma}_i \nabla V_i^-(x + c_i t) = \sqrt{\alpha_i \beta_i} \begin{pmatrix} -c_i \\ 1 \end{pmatrix} V_i^{-'}(x + c_i t), \end{aligned} \quad (2.7)$$

flowing along the characteristic lines, where $V_i^{+'}(s)$ and $V_i^{-'}(s)$ denote the derivatives of $V_i^+(s)$ and $V_i^-(s)$. It is clear that the currents do not interact and the potentials do not interact and, therefore, we can, in a sense, think of the medium as composed of two parallel independent sets of wires aligned with the characteristic directions (see Figure 1).

Clearly, the explicit expression of the d'Alembert solution (2.5), and therefore of (2.7), depends on the initial conditions chosen (see Section 2.2). For what concerns the boundary conditions we assume here that the medium is infinite with respect to x . (Later, in the numerical section, we will assume periodic boundary conditions in x .)

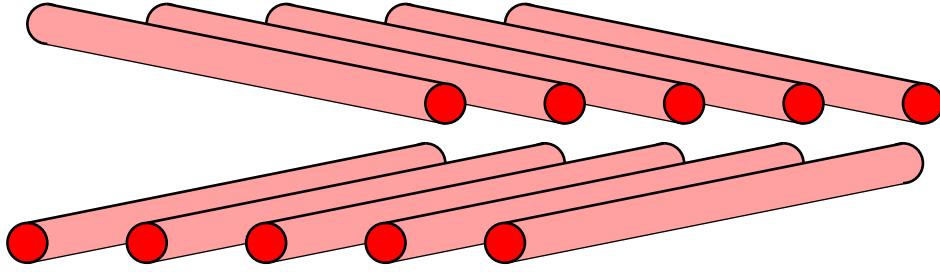


Figure 1: A hyperbolic medium can be thought as if it is composed of sets of unconnected wires, each set in the direction of the characteristics.

2.1 Transmission conditions at the interfaces

First of all, we recall that, in principle, the space-time distribution of the two materials is arbitrary, provided that the existence and uniqueness of the solution $V(x, t)$ is ensured. This places a constraint on the shape of the interfaces: each interface has to be such that there are always two incoming and two outgoing characteristics (see, for instance, [21]). To attain such a requirement, it is sufficient that the slope w of each interface in a space-time diagram fulfills the following relation [17]:

$$(w^2 - c_1^2)(w^2 - c_2^2) \geq 0. \quad (2.8)$$

In case of a pure spatial interface, that is, in case the interface is a vertical line in a space-time diagram, we have $w = 0$ and the above condition is trivially satisfied. Similarly, in case of a pure temporal interface, corresponding to a horizontal line in a space-time diagram, we have that $w \rightarrow \infty$ and once again condition (2.8) is trivially fulfilled.

For what concerns the transmission conditions for the potential across the interfaces, we require that the potential be continuous across each interface and such that the continuity of the current flux is preserved, i.e.,

$$V_1 = V_2 \quad (2.9)$$

$$\mathbf{n} \cdot \boldsymbol{\sigma}_1 \nabla V_1 = \mathbf{n} \cdot \boldsymbol{\sigma}_2 \nabla V_2, \quad (2.10)$$

with \mathbf{n} being the normal vector to the interface.

2.2 Initial conditions

Let us start by considering initial conditions of the type

$$V(x, 0) = H(x - a), \quad j_2(x, 0) = \delta(x - a)j_0, \quad (2.11)$$

and see how the corresponding disturbance propagates. Here $H(y)$ is the Heaviside function,

$$\begin{aligned} H(y) &= 0 & \text{if } y < 0, \\ &= 1 & \text{if } y > 0, \end{aligned} \quad (2.12)$$

and $\delta(y)$ is the Dirac delta function. Thus, we are injecting a total current flux j_0 at time $t = 0$ concentrated at $x = a$. In general, as illustrated in Figure 2, this generates a cascade of current lines branching as t increases that is difficult to analyze. If the process is ergodic, then one can probably understand the dynamics in an ensemble averaged sense, similarly to what is done in statistical physics.

2.3 Field Patterns

What is remarkable is that there are special space-time geometries, as illustrated in Figure 3 and Figure 4, where the dynamics is especially simple (note that the restriction (2.8) is trivially satisfied by both geometries having only horizontal and vertical interfaces). In particular, what causes the orderly pattern of characteristics in Figure 3 and in Figure 4 is the special relation between the characteristic lines and the geometry of the microstructure, as displayed

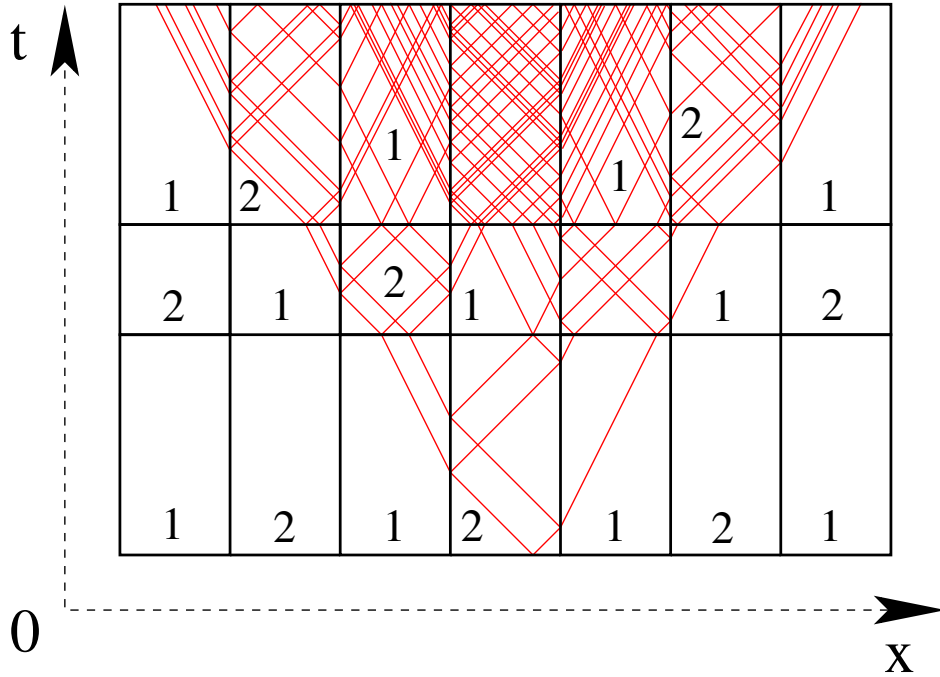


Figure 2: A typical dynamical process, showing a complicated cascade of current lines.

in Figure 5. From the configuration of the characteristic lines it is clear that, denoted with x_0 and t_0 the spatial and time dimensions of the unit cell of each space-time microstructure, their ratio reads

$$x_0/t_0 = \frac{c_1(c_1 + 2c_2)}{c_1 + c_2}, \quad (2.13)$$

for the geometry shown in Figure 3, and

$$x_0/t_0 = \frac{c_1(c_1 + 3c_2)}{2c_1 + c_2}, \quad (2.14)$$

for the microstructure presented in Figure 4. We will see that the dimensions of the unit cell of the space-time microstructure could be different from those of the unit cell of the network dynamics (for instance, for the microstructure in Figure 3, the former are x_0 and t_0 and the latter are $2x_0$ and t_0).

Note that by fixing the microgeometry we fix the volume fraction f of the space-time inclusions which, for the microstructure in Figure 3, is equal to $f = c_1c_2/[(c_1 + 2c_2)(c_1 + c_2)]$, while for the geometry in Figure 4 is equal to $f = c_1c_2/[(c_1 + 3c_2)(c_1 + c_2)]$.

3 Collections of field patterns as multidimensional or multicomponent objects

Let us begin by focusing on Figure 3, where the origin of the reference system $x = t = 0$ corresponds to the bottom left corner of an inclusion. The periodic pattern of characteristic lines that arises after a sufficiently large amount of time is totally determined by the sole index parameter ϕ , which is the distance between the bottom left corner of a specific inclusion and the intersection point between the base of that inclusion and the characteristic lines (see Figure 3). Note that for all the other inclusions struck by characteristic lines, such a distance is either ϕ or $c_2 - \phi$, where c_2 is the length of the base of the inclusion, if its height is set equal to one time unit. This is due to the fact that, for this space-time microstructure, the unit cell of the network dynamics (see also Figure 7 in the next Section) has length $2x_0$ and it contains two inclusions. Here, for simplicity, if we count the columns of inclusions starting from the right of the t -axis, those in an odd position will be parametrized by ϕ , whereas those in an even position by $c_2 - \phi$.

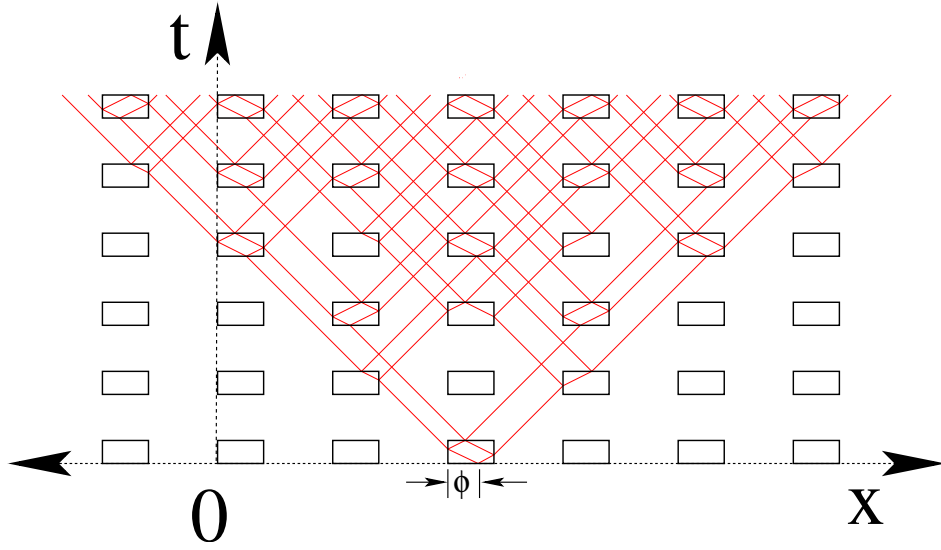


Figure 3: If the space-time geometry is suitably chosen, then the dynamics could be very simple and exhibit interesting features. For instance, here we show the case of a dynamic material composed of a matrix of material 1 with space-time rectangular inclusions of material 2. The distance between the inclusions is set in such a way that this periodic microstructure gives rise to a special orderly dynamics. The parameter ϕ is called the index parameter and it parameterizes the field pattern.

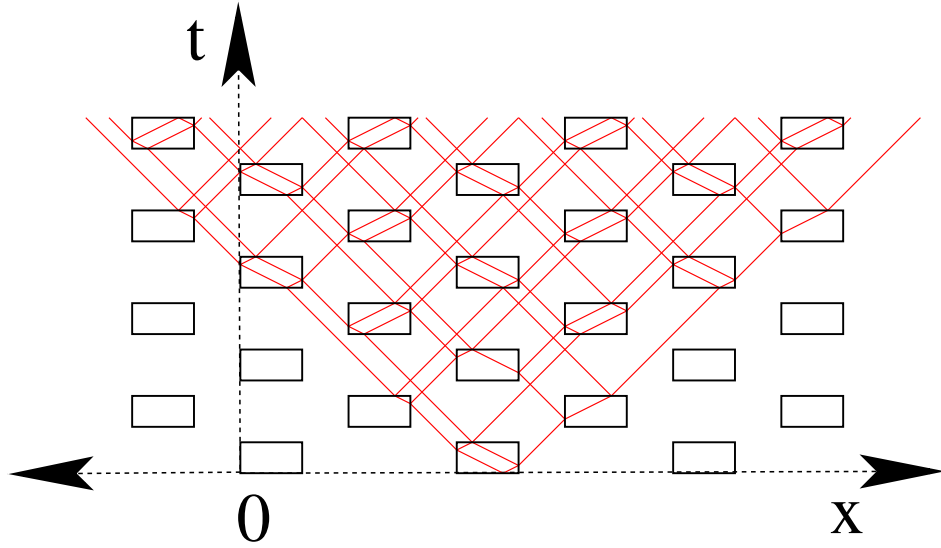


Figure 4: Also in the case where the space-time rectangular inclusions are staggered (and not aligned as in the case shown in Figure 3), the dynamics is very simple.

Notice that the index parameter ϕ determines in a unique way the periodic pattern of characteristic lines that arises after a sufficiently large amount of time, as it is not related to the specific initial conditions chosen: the ϕ -field pattern in Figure 3 can indeed be obtained in different ways and each way will have a different current distribution. For instance, in Figure 6a the same ϕ -field pattern of Figure 3 is launched by injecting current at a point $(a, 0)$ belonging to the matrix, whereas in Figure 6b it is launched by injecting current at three points at a different time (note that in this figure the reference system is different from the one in Figure 3). We will see in Section 6 that some patterns parametrized by the same parameter ϕ blow up in time, while others have a wave-like behavior which does not blow up.

If the initial conditions are suitably chosen, more than one field pattern can be launched. This gives rise to

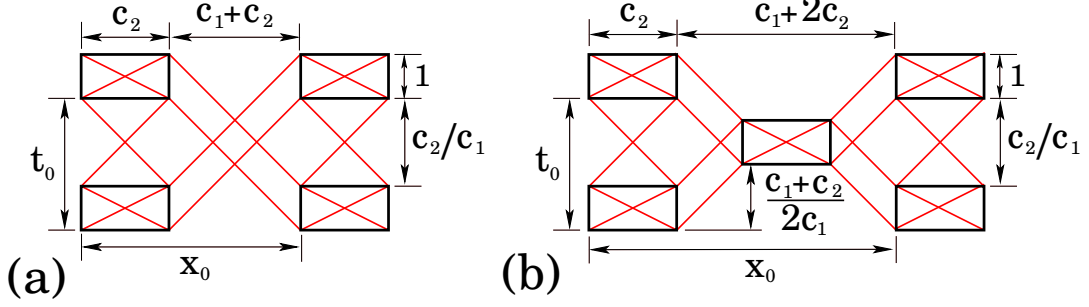


Figure 5: The simplicity of the dynamics related to the space-time microstructures with aligned (Figure 3) and staggered (Figure 4) rectangular inclusions results from the specific geometrical structure of the two materials, as can be seen here, where the red lines denote characteristic lines.

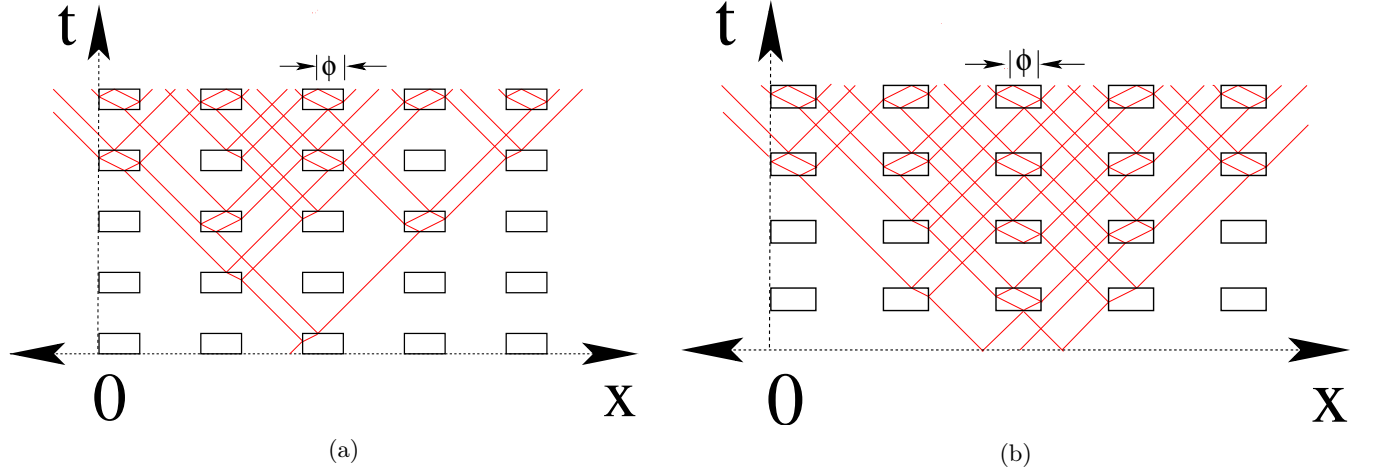


Figure 6: The field pattern of Figure 3, indexed by the parameter ϕ , can be obtained, for a sufficient large amount of time, also by considering initial conditions different from (4.11). In Figure 6a the reference system is the same as in Figure 3 but the point of injection of current flux now belongs to the matrix, whereas in Figure 6b the ϕ -field pattern is recovered by injecting current flux at three points in a different reference system. Note that these different launching conditions give rise to different current distributions within the field pattern.

a collection of field patterns, each one parametrized by its index parameter ϕ_i , with $i = 1, 2, \dots, m$, m being the number of field patterns launched. For instance, pick two parameters ϵ_1 and ϵ_2 lying between 0 and 1, and choose real amplitudes s_1 , s_2 , j_1 , and j_2 . Then, the initial conditions

$$\begin{aligned} V(x, 0) &= s_1 H(x - 2x_0(l + \epsilon_1)) + s_2 H(x - 2x_0(n + \epsilon_2)), \\ j_2(x, 0) &= \delta(x - 2x_0(l + \epsilon_1))j_1 + \delta(x - 2x_0(n + \epsilon_2))j_2, \end{aligned} \quad (3.1)$$

where l and n are integers, can launch anywhere from one to four field patterns in the space-time microstructure of Figure 3, depending on the value of the parameters ϵ_1 and ϵ_2 . Suppose, first, that the points where the current is injected, $(x, t) = (2x_0(l + \epsilon_1), 0)$ and $(x, t) = (2x_0(n + \epsilon_2), 0)$, lie at the base of inclusions. If they both belong to inclusions in odd columns, we have $\epsilon_i < c_2/(2x_0) = c_2/(2(c_1 + 2c_2))$, whereas if they both belong to an inclusion in an even column we have $1/2 < \epsilon_i < 1/2 + c_2/(2x_0) = 1/2 + c_2/(2(c_1 + 2c_2))$. In both cases, two field patterns can be launched and the associated index parameters ϕ_1 and ϕ_2 are easily identified as $\phi_i = 2\epsilon_i x_0 = 2\epsilon_i(c_1 + 2c_2)$, in the first case, and $c_2 - \phi_i = 2\epsilon_i x_0 - x_0 = (2\epsilon_i - 1)(c_1 + 2c_2)$, in the second case. Note that if $\phi_1 = \phi_2$ then only one field pattern is generated. Finally, if $c_2/(2(c_1 + 2c_2)) < \epsilon_i < 1/2$ or $\epsilon_i > 1/2 + c_2/(2(c_1 + 2c_2))$, then the points $(x, t) = (2x_0(l + \epsilon_1), 0)$ and $(x, t) = (2x_0(n + \epsilon_2), 0)$ belong to the matrix and there could be up to four associated field patterns: the index parameters are found by tracing the relevant characteristic or characteristics that originate from the source at $t = 0$ until they strike the base of an inclusion.

Collections of field patterns are especially interesting because of their multidimensional nature. They are similar in some respects to non-interacting particles in quantum mechanics. The idea is that one can split the space-time diagram into an infinite number of disjoint “conducting networks” that do not interact. Each field pattern in a collection then lives on one of these conducting networks.

Consider a collection of m field patterns, parameterized by the index parameters $\phi_1, \phi_2, \dots, \phi_m$. The potential $V_i(x, t)$ associated with the field pattern with index ϕ_i satisfies the wave equation and, by the superposition principle and the linearity of the problem, also the total potential

$$V(x, t) = \sum_{i=1}^m V_i(x, t), \quad (3.2)$$

satisfies the wave-equation. Although the dynamics of $V(x, t)$ is governed by the wave equation, it is far simpler to track the dynamics of $V_i(x, t)$ for each field pattern, $i = 1, 2, \dots, m$, since the field patterns do not interact. We can think of $V_i(x, t)$ as living in its separate dimension, x_i , and rather than considering the potential $V(x, t)$ one can consider the multidimensional potential

$$V(x_1, x_2, \dots, x_m) = \sum_{i=1}^m V_i(x_i, t). \quad (3.3)$$

This multidimensional potential is more suitable for capturing the dynamics than the underlying potential $V(x, t)$. It is expected that one will be able, in appropriate conditions, to homogenize the behavior of field patterns so that $V_i(x_i, t)$ is replaced by some suitably defined "coarse grained" potential $\underline{V}_i(x_i, t)$ that captures the macroscopic modulation of $V_i(x_i, t)$ and that satisfies an appropriate homogenized equation (still to be found). While one could speak about the dynamics of the multidimensional coarse grained potential

$$\underline{V}(x_1, x_2, \dots, x_m) = \sum_{i=1}^m \underline{V}_i(x_i, t), \quad (3.4)$$

there would be no suitable equation to describe the dynamics of the coarse grained potential

$$\underline{V}(x, t) = \sum_{i=1}^m \underline{V}_i(x, t), \quad (3.5)$$

since too much information is lost in taking this last sum.

An alternative to introducing these extra dimensions is to introduce a vector potential $\mathbf{V}(x, t)$ with m components $V_i(x, t)$. With coarse grained potentials $\underline{V}_i(x, t)$ the macroscopic behavior of the collection of noninteracting field patterns is then governed by the vector potential $\underline{\mathbf{V}}(x, t)$ having these potentials as components. If we think of these field patterns as living on separate "conducting networks" then, in the presence of interactions (caused by small nonlinearities or a small imaginary part of $\sigma(x, t)$) the work of Khruslov [59] and Briane [60, 61] (see also [41] where related ideas are embodied in a quantum mechanical context) suggests that the homogenized equations may simply couple these field components. If this turns out to be the case then the full multivariate potential $\underline{V}(x_1, x_2, \dots, x_m)$ may not be needed.

4 Solving the cell problem

In this Section we aim at making steps towards determining the effective properties of the material having the space-time microstructure shown in Figure 3. The results concerning the microgeometry in Figure 4 are given in the supplementary material, as they are very similar to those presented here. We will just be concentrating on the case where the fields $\mathbf{e}(\mathbf{x})$ and $\mathbf{j}(\mathbf{x})$ have the same periodicity as the field pattern, i.e., their cell of periodicity contains two inclusions.

As already noticed in the previous section, the special geometry in Figure 3 is such that the characteristic lines follows a certain periodic pattern. Let us consider, then, the unit cell for the network dynamics (see Figure 7) (note that the size of such a unit cell is twice the size of the unit cell of the space-time microstructure, that is, $2x_0$ and t_0) and let us determine the solution of the problem on the unit cell in the case the initial conditions are

$$V_i(x, 0) = \frac{j_0}{c_i \beta_i} H(x), \quad j_2(x, 0) = j_0 \delta(x). \quad (4.1)$$

Consequently, the potentials $V_i^+(x, t)$ and $V_i^-(x, t)$ in phase i take the following expressions:

$$V_i^+(x, t) = a_i^+[1 - H(x - c_it)], \quad V_i^-(x, t) = a_i^-H(x + c_it) \quad (4.2)$$

with $a_i^+ = -j_0/(c_i\beta_i) = -a_i^-$. The associated currents, according to (2.7), are

$$\begin{aligned} \mathbf{j}_i^+ &= a_i^+ \sqrt{\alpha_i\beta_i} \begin{pmatrix} c_i \\ 1 \end{pmatrix} \delta(x - c_it) \equiv \frac{a_i^+}{\gamma_i} \frac{1}{\sqrt{1 + c_i^2}} \begin{pmatrix} c_i \\ 1 \end{pmatrix} \delta(x - c_it), \\ \mathbf{j}_i^- &= a_i^- \sqrt{\alpha_i\beta_i} \begin{pmatrix} -c_i \\ 1 \end{pmatrix} \delta(x + c_it) \equiv \frac{a_i^-}{\gamma_i} \frac{1}{\sqrt{1 + c_i^2}} \begin{pmatrix} -c_i \\ 1 \end{pmatrix} \delta(x - c_it), \end{aligned} \quad (4.3)$$

where

$$\gamma_i = \frac{1}{\sqrt{\alpha_i(\alpha_i + \beta_i)}}. \quad (4.4)$$

These currents flowing along the characteristics have magnitudes $j_i^+ = a_i^+ \gamma_i$ and $j_i^- = a_i^- \gamma_i$ in the direction of positive time. Bearing this remark in mind, since the jumps in the potential across the characteristics in the direction of positive time are of magnitude a_i^+ and a_i^- (see (4.2)), then we can conclude that the constants γ_1 and γ_2 relate the potential jumps across the characteristic lines to the current flowing through them.

We highlight the fact that the case analyzed in detail in this section is of particular interest as the solution of such a problem can be used as the starting point to build the solutions corresponding to the choice of other initial conditions, as also shown in Section 5, where, instead of a prescribed jump in potential at $t = 0$, we consider the case of a linear potential.

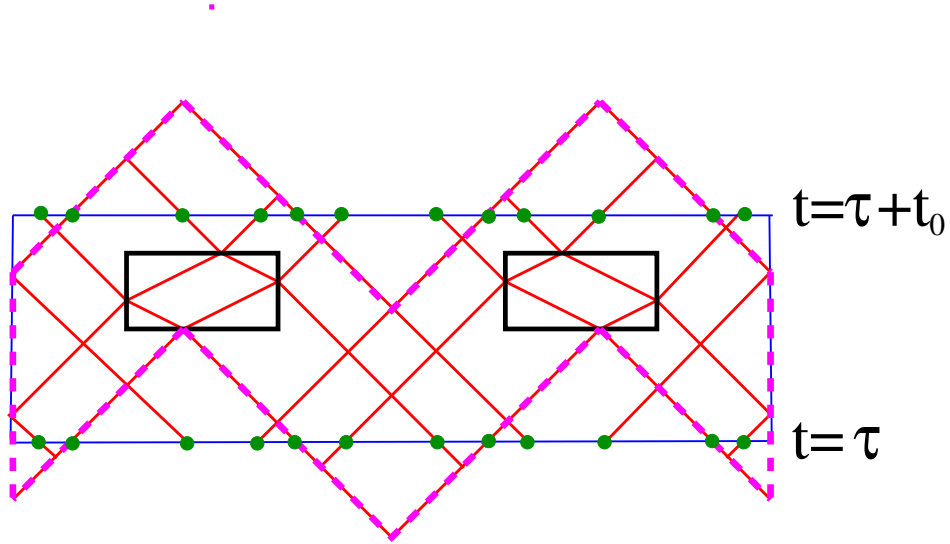


Figure 7: Outlined by the purple dashed lines is the unit cell of periodicity for the dynamics of the microgeometry shown in Figure 3 in the case of a periodic field pattern. The red lines denote characteristic lines. The current flows along such lines and, across them, there is a jump in potential. Note that the dynamics splits into dynamics that are symmetric and antisymmetric with respect to reflection about the vertical centerline of the cell. We call these the symmetric dynamics and the antisymmetric dynamics. If the field pattern is not periodic then we can still consider a periodic array of the characteristic lines, and the period cell could be taken to be that outlined in blue. Current injected at time $t = \tau$ at any of the 12 points marked by the green dots at the bottom of the unit cell can contribute towards the excitation of the same field pattern. This current exits the unit cell at time $t = \tau + t_0$ at any of the 12 points marked by the green dots at the top of the unit cell, and may flow to the exit points of adjoining unit cells as well.

The symmetry of the unit cell with respect to the vertical centerline suggests the idea of splitting the dynamics represented in Figure 7 into dynamics that are symmetric and dynamics that are antisymmetric: every type of dynamics can be recovered by suitably choosing the linear combination between these two elementary cases.

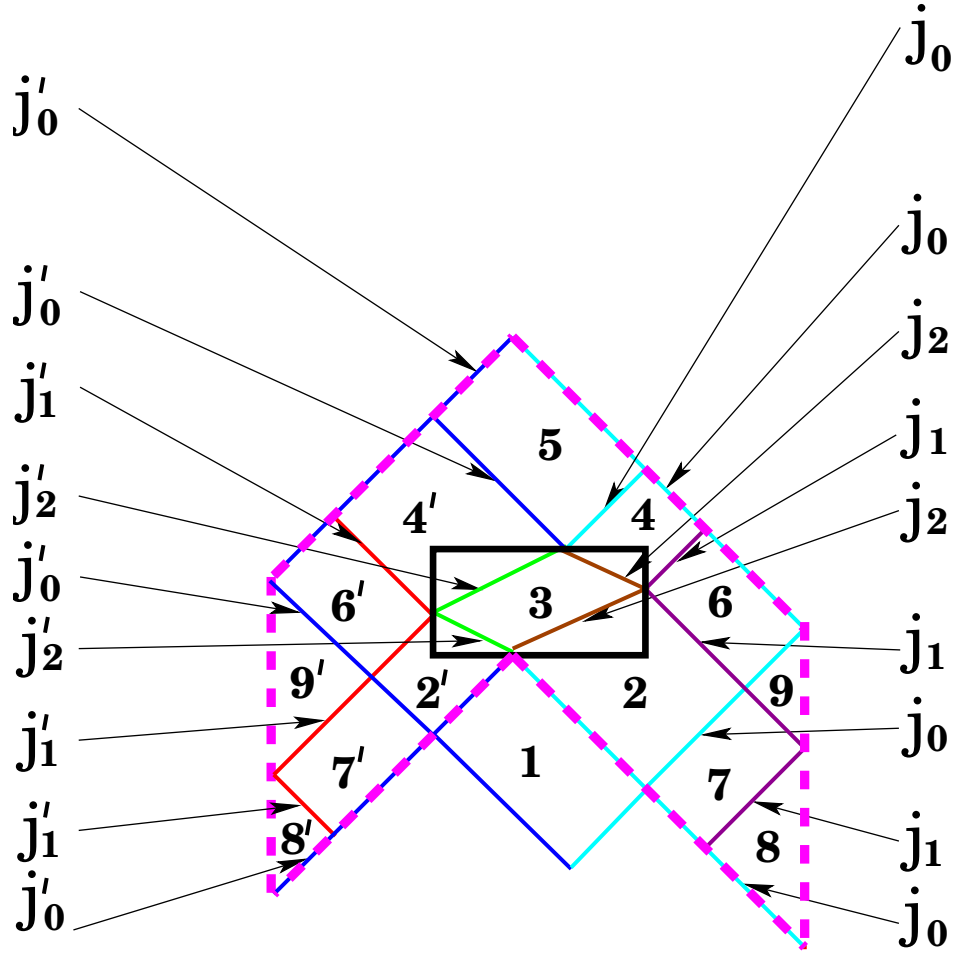


Figure 8: The current flows in one half of the unit cell for symmetric dynamics. Here different colors are used to distinguish lines that have different currents flowing along them. Periodicity and symmetry ensure that the currents flow as described in this figure.

4.1 Symmetric dynamics

To solve for the currents and potentials associated with the symmetric dynamics with periodic currents (and hence periodic electric fields), we suppose all the currents are flowing in the direction of positive time, and have the magnitudes j_0, j_1, j_2 and j'_0, j'_1, j'_2 as indicated on the lines in Figure 8. Periodicity and symmetry ensure the current flow has this structure. By conservation of current at the interfaces between the phases (see equation (2.10)), we require that

$$j_0 + j'_0 = j_2 + j'_2. \quad (4.5)$$

Notice that, since the potential is piecewise constant, the condition of continuity given by (2.9) is trivially satisfied.

With reference to Figure 8, we let $V_i, i = 1, 2, \dots, 9$ denote the potentials in each of the regions 1, 2, \dots , 9 and we let $V'_i, i = 2, 4, 6, 7, 8, 9$ denote the potentials in each of the regions 2', 4', 6', 7', 8', 9'. For simplicity, we set $V_1 = 0$. Then, from the aforementioned rule that the potential jump across a characteristic line is γ_i times the current flowing through it, we obtain successively

$$\begin{aligned} V_2 &= \gamma_1 j_0, & V'_2 &= \gamma_1 j'_0, & V_3 &= \gamma_1 j_0 + \gamma_2 j_2 = \gamma_1 j'_0 + \gamma_2 j'_2, & V_6 &= \gamma_1 (j_0 + j_1), & V'_6 &= \gamma_1 (j'_0 + j'_1), \\ V_4 &= \gamma_1 j_0 + 2\gamma_2 j_2 = \gamma_1 (j_0 + 2j_2), & V'_4 &= \gamma_1 j'_0 + 2\gamma_2 j'_2 = \gamma_1 (j'_0 + 2j'_2), & V_7 &= 0, & V'_7 &= 0, \\ V_5 &= 2\gamma_1 j_0 + 2\gamma_2 j_2 = 2\gamma_1 j'_0 + 2\gamma_2 j'_2, & V_8 &= -\gamma_1 j_1, & V'_8 &= -\gamma_1 j'_1, & V_9 &= \gamma_1 j_1, & V'_9 &= \gamma_1 j'_1. \end{aligned} \quad (4.6)$$

Thus, in addition to (4.5), we are left with the 3 constraints

$$\gamma_1 j_0 + \gamma_2 j_2 = \gamma_1 j'_0 + \gamma_2 j'_2, \quad \gamma_2 j_2 = \gamma_1 j_1, \quad \gamma_2 j'_2 = \gamma_1 j'_1, \quad (4.7)$$

which incidentally imply that $j_0 + j_1 = j'_0 + j'_1$, as can be seen by multiplying the first formula in (4.7) by γ_1 . So all the currents can be expressed in terms of only two independent currents, say j_0 and j'_0 . Then,

$$\begin{aligned} j_2 &= \frac{1}{2}(j_0 + j'_0) - \frac{\gamma_1}{2\gamma_2}(j_0 - j'_0), & j_1 &= \gamma_2 j_2 / \gamma_1, \\ j'_2 &= \frac{1}{2}(j_0 + j'_0) + \frac{\gamma_1}{2\gamma_2}(j_0 - j'_0), & j'_1 &= \gamma_2 j'_2 / \gamma_1. \end{aligned} \quad (4.8)$$

The advantage of studying the symmetric dynamics in Figure 8, rather than the general dynamics in Figure 7, lies in the fact that the symmetry with respect to the centerline of the unit cell leads to average current fields and average electric fields that have non-zero components only in the time direction. In particular, the average current field is easily worked out from the flux of current into the lower boundary of the cell of Figure 8, and is $(2j_0 + 2j'_0 + j_1 + j'_1)/x_0$ in the time direction. The average electric field is easily worked out from the potential jump across the cell in the vertical direction, and is $(V_1 - V_5)/t_0$. The ratio of the average current field divided by the average electric field is

$$\begin{aligned} \frac{(2j_0 + 2j'_0 + j_1 + j'_1)/x_0}{(V_1 - V_5)/t_0} &= -\frac{t_0(j_0 + j'_0)[2 + (\gamma_2/\gamma_1)]}{x_0(2\gamma_1 j_0 + 2\gamma_2 j_2)} = -\frac{t_0(j_0 + j'_0)[2 + (\gamma_2/\gamma_1)]}{x_0(\gamma_1 j_0 + \gamma_2 j_0 + \gamma_1 j'_0 + \gamma_2 j'_0)} \\ &= -\frac{t_0[2 + (\gamma_2/\gamma_1)]}{x_0(\gamma_1 + \gamma_2)} \end{aligned} \quad (4.9)$$

and this corresponds to the effective conductivity coefficient in the time direction, that is, $-\beta_*$.

4.2 Antisymmetric dynamics

To solve for the currents and potentials associated with the antisymmetric dynamics with periodic currents (and hence periodic electric fields), we assign the convention that currents flowing in the direction of positive time have positive sign, and currents flowing in the direction of negative time have negative sign. The currents are labelled j_0, j_1, j_2 and j'_0, j'_1, j'_2 on the lines in Figure 9. Periodicity and antisymmetry ensure the current flow has this structure. By conservation of current at the interfaces between the phases (see equation (2.10)) we require that

$$j_0 + j'_0 = j_2 + j'_2, \quad j_1 = j_2, \quad j'_1 = j'_2. \quad (4.10)$$

We let $V_i, i = 1, 2, \dots, 9$ denote the potentials in each of the regions 1, 2, \dots , 9 and we let $V'_i, i = 2, 4, 6, 7, 8, 9$ denote the potentials in each of the regions 2', 4', 6', 7', 8', 9'. Once again, for simplicity, we set $V_1 = 0$. Then, from the rule that the potential jump across a characteristic line is γ_i times the current flowing through it, we obtain successively

$$\begin{aligned} V_2 &= \gamma_1 j_0, & V'_2 &= \gamma_1 j'_0, & V_3 &= \gamma_1 j_0 + \gamma_2 j_2 = \gamma_1 j'_0 + \gamma_2 j'_2, & V_6 &= \gamma_1(j_0 - j_1), \\ V'_6 &= \gamma_1(j'_0 - j'_1), & V_4 &= \gamma_1 j_0, & V'_4 &= \gamma_1 j'_0, & V_5 &= 0, & V_7 &= 0, & V'_7 &= 0, \\ V_8 &= -\gamma_1 j_1, & V'_8 &= -\gamma_1 j'_1, & V_9 &= -\gamma_1 j_1, & V'_9 &= -\gamma_1 j'_1. \end{aligned} \quad (4.11)$$

So in addition to (4.5) the currents must satisfy the constraint

$$\gamma_1 j_0 + \gamma_2 j_2 = \gamma_1 j'_0 + \gamma_2 j'_2. \quad (4.12)$$

Thus j_0 , and j'_0 can be chosen independently, and in terms of these

$$\begin{aligned} j_1 = j_2 &= \frac{1}{2}(j_0 + j'_0) - \frac{\gamma_1}{2\gamma_2}(j_0 - j'_0), \\ j'_1 = j'_2 &= \frac{1}{2}(j_0 + j'_0) + \frac{\gamma_1}{2\gamma_2}(j_0 - j'_0). \end{aligned} \quad (4.13)$$

As $V_5 = V_1$ there is no average electric field in the vertical direction. Similarly, there is no current field in the vertical direction. In the horizontal direction, by looking at the current flux out of the unit cell, one sees the average current

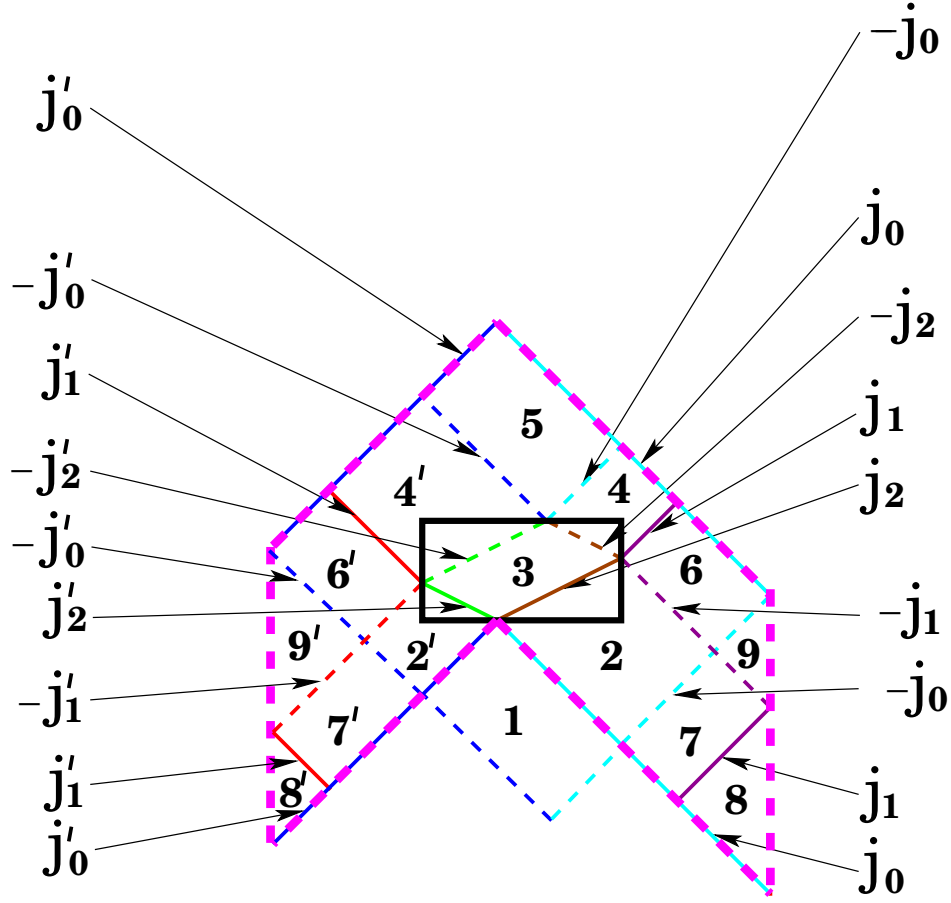


Figure 9: The current flows in one half of the unit cell for antisymmetric dynamics. Here different colors are used to distinguish lines that have different currents flowing along them, and dashed lines indicate currents that are measured with respect to decreasing time: thus a current j_i flowing in the direction of decreasing time corresponds to a current $-j_i$ in the direction of increasing time. Periodicity and antisymmetry ensure that the currents flow as described in this figure.

to the right is $2(j_1 - j_0)/t_0$. The average electric field pointing to the right is $(V'_9 - V_9)/x_0$. The ratio of the average current field divided by the average electric field is then

$$\frac{2(j_1 - j_0)/t_0}{(V'_9 - V_9)/x_0} = \frac{2x_0(j_1 - j_0)}{t_0\gamma_1(j_1 - j'_1)} = \frac{x_0(j_0 - j'_0)(\gamma_1 + \gamma_2)}{t_0\gamma_1^2(j_0 - j'_0)} = \frac{x_0(\gamma_1 + \gamma_2)}{t_0\gamma_1^2}, \quad (4.14)$$

and this corresponds to the effective conductivity coefficient in the space direction, α_* .

Therefore, from (2.13), (4.9), and (4.14) we see that the "effective conductivity tensor" is

$$\sigma_* = \begin{pmatrix} \alpha_* & 0 \\ 0 & -\beta_* \end{pmatrix} = \begin{pmatrix} \frac{x_0(\gamma_1 + \gamma_2)}{t_0\gamma_1^2} & 0 \\ 0 & -\frac{t_0[2 + (\gamma_2/\gamma_1)]}{x_0(\gamma_1 + \gamma_2)} \end{pmatrix} = \begin{pmatrix} \frac{c_1(c_1 + 2c_2)(\gamma_1 + \gamma_2)}{\gamma_1^2(c_1 + c_2)} & 0 \\ 0 & -\frac{(c_1 + c_2)[2 + (\gamma_2/\gamma_1)]}{c_1(c_1 + 2c_2)(\gamma_1 + \gamma_2)} \end{pmatrix}. \quad (4.15)$$

The associated "effective speed" is therefore

$$c_* = \sqrt{\alpha_*/\beta_*} = \frac{c_1(c_1 + 2c_2)(\gamma_1 + \gamma_2)}{c_1 + c_2} \sqrt{\frac{1}{\gamma_1(2\gamma_1 + \gamma_2)}}. \quad (4.16)$$

Interestingly, this does not approach the wave velocity c_1 , even when the parameters of phase 2 approach those of phase 1. If we had chosen our units of space and time so that $x_0 = 1$ and $t_0 = 1$ then the corresponding dimensionless

speed would be

$$\frac{c_* t_0}{x_0} = (\gamma_1 + \gamma_2) \sqrt{\frac{1}{\gamma_1(2\gamma_1 + \gamma_2)}}. \quad (4.17)$$

We have put quotes around "effective conductivity tensor" and "effective speed" because at this stage it is unclear what is their physical significance. If the conductivity tensor field $\sigma(\mathbf{x})$ had a very tiny imaginary part (as relevant to composites of hyperbolic materials, when $\sigma(\mathbf{x})$ is replaced by the dielectric tensor field $\varepsilon(\mathbf{x})$, and time is replaced by a spatial variable) then indeed σ_* would be the appropriate "speed" giving the effective "characteristic lines" of propagation. In the absence of such an imaginary part one needs to derive the appropriate homogenized equations. This homogenized equation is unlikely to be simply $\nabla \cdot \sigma_* \nabla V = 0$ where $V(\mathbf{x})$ is some coarse grained potential, as it is quite evident from the branching nature of field patterns (see Figure 3 and Figure 4) that there should be some term giving dispersion in the effective equations.

5 Associated field patterns

As before let us assume the origin $x = t = 0$ coincides with the bottom left corner of an inclusion, as in Figure 3. Now given a non-negative index parameter $\phi < c_2$, suppose we launch a field pattern $V(x, t)$ by setting the initial conditions

$$V(x, 0) = H(x - \phi), \quad j_2(x, 0) = -\sqrt{\alpha_2 \beta_2} \delta(x - \phi), \quad (5.1)$$

so that initially the discontinuity just propagates to the right: in the inclusion containing the origin, the potential $V(x, t)$ is just equal to $H(x - \phi - c_2 t)$ until the time $1 - \phi/c_2$ when the discontinuity strikes the right hand side of the inclusion. Let us label this potential $V(x, t, \phi)$ and its associated current $\mathbf{j}(x, t, \phi)$ to make explicit the dependence on ϕ . Now given two index parameters ϕ_1 and ϕ_2 , where $0 < \phi_1 < \phi_2 < c_2$, we can consider the potential

$$W(x, t, \phi_1, \phi_2) = \int_{\phi_1}^{\phi_2} V(x, t, \phi) d\phi. \quad (5.2)$$

This function $W(x, t, \phi_1, \phi_2)$ is clearly a solution of the wave equation being a superposition of solutions. It has discontinuities in slope along the lines indicated in Figure 10. Let the associated current field be labelled $\mathbf{J}(x, t, \phi_1, \phi_2)$.

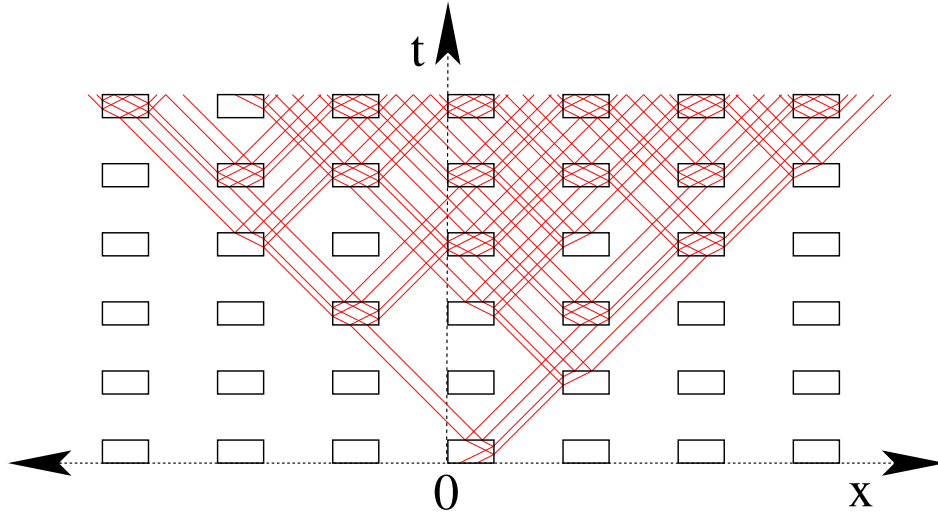


Figure 10: Evolution of the lines of discontinuity of slope of the associated field pattern $W(x, t, \phi_1, \phi_2)$

It is given by

$$\mathbf{J}(x, t, \phi_1, \phi_2) = -\sigma(x, t) \nabla W(x, t, \phi_1, \phi_2) = \int_{\phi_1}^{\phi_2} \mathbf{j}(x, t, \phi) d\phi. \quad (5.3)$$

Clearly then, $W(x, t)$ satisfies the initial conditions,

$$\begin{aligned}
W(x, 0, \phi_1, \phi_2) &= \int_{\phi_1}^{\phi_2} H(x - \phi) d\phi = 0 \quad \text{if } x < \phi_1 \\
&= x - \phi_1 \quad \text{if } \phi_1 < x < \phi_2 \\
&= \phi_2 - \phi_1 \quad \text{if } x > \phi_2, \\
J_2(x, 0, \phi_1, \phi_2) &= -\sqrt{\phi_2 \beta_2} \int_{\phi_1}^{\phi_2} \delta(x - \phi) d\phi = 0 \quad \text{if } x < \phi_1 \\
&= -\sqrt{\phi_2 \beta_2} \quad \text{if } \phi_1 < x < \phi_2 \\
&= 0 \quad \text{if } x > \phi_2,
\end{aligned} \tag{5.4}$$

By considering the evolution of this disturbance, it is clear that the associated field pattern $W(x, t, \phi_1, \phi_2)$ is a linear function of x and t in each space-time polygonal region with boundaries marked by the lines of discontinuity in slope in Figure 10. Thus the lines of discontinuity in the associated field pattern can be considered as sources and sinks of the "electric field" $-\partial W(x, t, \phi_1, \phi_2)/\partial x$, like electrical charges. We call $W(x, t, \phi_1, \phi_2)$ an associated field pattern of the first degree. An example of an associated field pattern of the first degree that is periodic is graphed in Figure 11

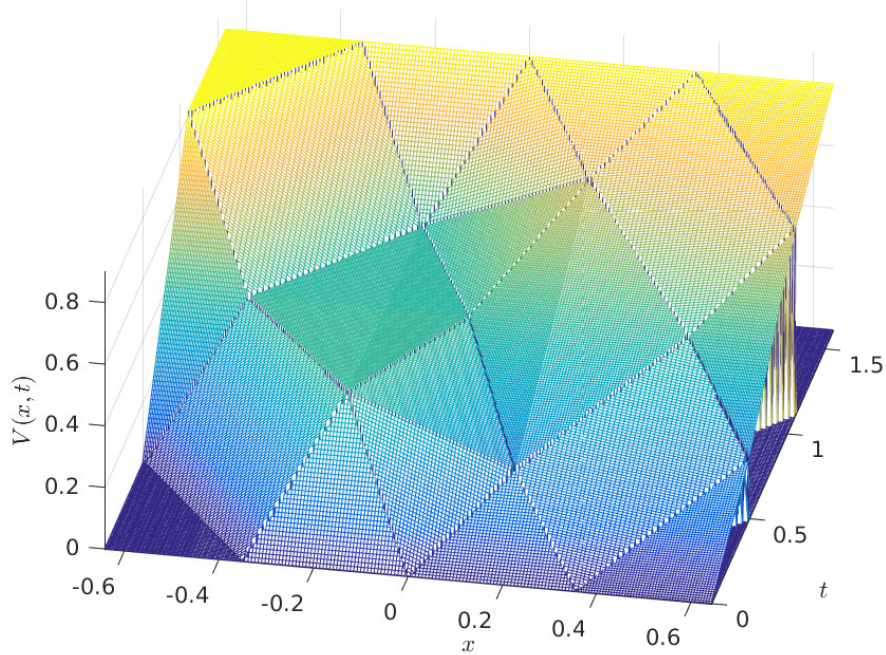


Figure 11: An associated field pattern, with extreme values $\phi_1 = 0$ and $\phi_2 = c_2$, that is generated from the symmetric periodic potentials $V(x, t, \phi)$ given in Section 3.2, with parameter choices $\alpha_1 = 0.5, \beta_1 = 1.5, \alpha_2 = 1$, and $\beta_2 = 8$, corresponding to $\gamma_1 = 1$ and $\gamma_2 = 3$, and with currents $j_0 = 0.5$, and $j'_0 = 1$. Note the piecewise linear nature of the potential. The spurious vertical lines at the right back side are a numerical artifact and should be ignored.

An associated field pattern of the second degree would be the function

$$Y(x, t, \phi_{11}, \phi_{12}, \phi_{21}, \phi_{22}) = \int_{\phi_{11}}^{\phi_{12}} d\phi_1 \int_{\phi_{21}}^{\phi_{22}} d\phi_2 W(x, t, \phi_1, \phi_2). \tag{5.5}$$

where $\phi_{11}, \phi_{12}, \phi_{21}$, and ϕ_{22} are parameters such that

$$0 < \phi_{11} < \phi_{12} < \phi_{21} < \phi_{22} < c_2. \tag{5.6}$$

This function $Y(x, t, \phi_{11}, \phi_{12}, \phi_{21}, \phi_{22})$ will have discontinuities in its second derivatives across the lines in the field pattern. Field patterns of higher degree can then be defined in the obvious way.

6 Numerical results

To test the theoretical results obtained in Section 4.1 and explore the subject of field patterns further, we perform some numerical analyses. Since a field pattern lives on its own discrete network, it is only necessary to study the dynamics of field patterns on these discrete networks. On each discrete network the evolution of the currents in the "wires" can be viewed as a dynamical system, and due to the periodicity in time it suffices to study the currents in the "wires" at times $t = \tau + n t_0$ for $n = 0, 1, 2, \dots$, where τ is some fixed time. To simplify the description we choose τ to be a time where none of the "wires" in the discrete network intersect, as shown for example by the horizontal line at $t = \tau$ in Figure 7. Then the state of the system at these discrete times is entirely determined by specifying the currents in each of the "wires": it is captured by the function $j(k, m, n)$ where k , taking integer values between 1 and 12 indexes the "wires" in each unit cell, the integer m indexes the cell, and the integer n indexes the discrete time. The state at any intervening time between the discrete times is easily determined from the dynamics: we can think of the set of currents at the discrete times as being representative of the full dynamics in much the same way that a Poincaré map helps one visualize the dynamics of a dynamical system.

Our aim is to determine the evolution of the state function $j(k, m, n)$, as $n = 0, 1, 2, \dots$, which is representative of the time, increases. To achieve such a goal, we calculate the Green function that allows one to recover the currents at a certain time $t = \tau + n t_0$ with n fixed, given the currents at time $t = \tau + (n - 1) t_0$. Clearly, this is done by taking one unit cell, say with $m = m_0$ and injecting, at $t = \tau$ ($n = 0$), a unitary current in each of the 12 points $k = 1, 2, \dots, 12$ marked by the green dots on the line $t = \tau$ in Figure 7, one at a time, and by calculating how such a current flows along the characteristic lines to determine the currents at $t = \tau + t_0$ ($n = 1$). Note that the current injected in some of the 12 points may cross the boundary of the unit cell: if one injects, for instance, a current at point 1, this will flow towards the points 9, 10 and 12 of the adjacent cell on the left, having $m = m_0 - 1$, whereas, if one injects current at point 12, for example, this will flow towards the points 1, 3 and 4 of the adjacent cell on the right, having $m = m_0 + 1$. This means that the currents injected in a unit cell at $t = \tau$ ($n = 0$) may influence at $t = \tau + t_0$ ($n = 1$), the currents in up to three unit cells.

The Green function so calculated, then, can be denoted by $G_{k,k'}(m - m')$ to indicate that it provides the current at point k , with $k = 1, 2, \dots, 12$, of cell m , given the current at point k' , with $k' = 1, 2, \dots, 12$, of cell m' . Such a function obviously only depends on the differences $m - m'$, and its explicit expression is given in Section 8. Then, the current at the point k of cell m at time $t = \tau + n t_0$ is determined by the currents at points k' of cells m' at the previous time $t = \tau + (n - 1) t_0$ by

$$j(k, m, n) = \sum_{k', m'} T_{(k, m), (k', m')} j(k', m', n - 1), \quad (6.1)$$

where

$$T_{(k, m), (k', m')} = G_{k, k'}(m - m') \quad (6.2)$$

is the transfer matrix. To approximate the hypothesis of an infinite medium in the x direction we could consider a very large number M of cells. It is then natural to take periodic boundary conditions, so that we can think of the discrete network as lying on the surface of a cylinder, with the axis variable corresponding to time and the angle variable corresponding to space. Thus in (6.1) cell M is identified with cell 0 and cell -1 is identified with cell $M - 1$: equivalently the argument $m - m'$ of $G_{k, k'}(m - m')$ in (6.1) should be replaced with $(m - m') \bmod M$.

6.1 On testing the periodic dynamics

To test the periodic solution corresponding to the symmetric dynamics that we derived in the previous section, we have just to impose that, at $t = \tau$, the distribution of currents in the 12 points of each unit cell be equal to the periodic distribution of currents given by the symmetric dynamics of Figure 8, and check that for $n = 1, 2, \dots$, such a distribution does not change. In Figure 12 we represent the time evolution of the currents for $n = 0, 1, \dots, 100$ in 10 cells (so that the total number of points is 120), for the case when $j_0 = 1$ and $j'_0 = -2$, and $\gamma_1 = 1$ and $\gamma_2 = 3$. As expected, the solution depicted in Figure 12 is clearly periodic both in space and time.

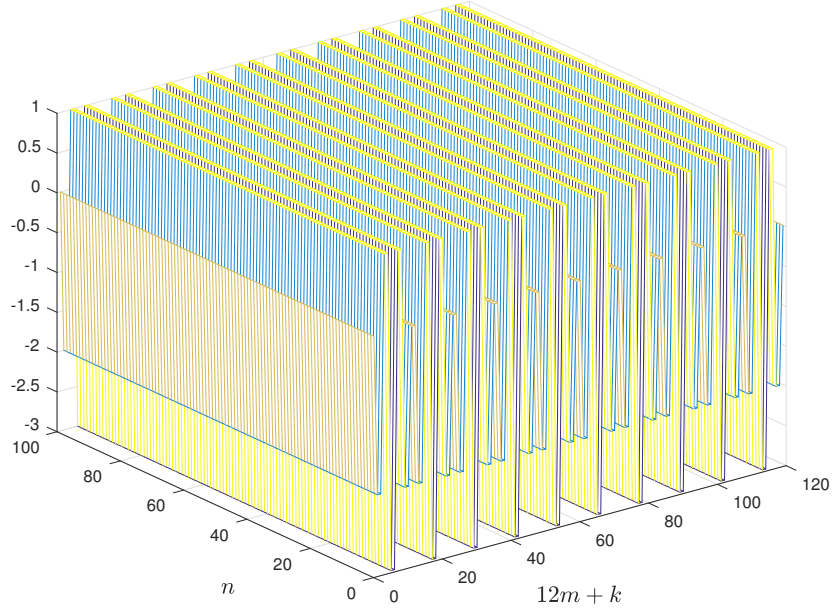


Figure 12: Evolution of the currents flow in 10 cells (since there are 12 test points in each cell, the total number of points monitored is equal to 120), for $t = \tau + nt_0$ with $n = 0, 1, \dots, 100$, in the case when the distribution of currents injected at $t = \tau$ ($n = 0$) is equal to the periodic distribution given by the symmetric dynamics of Figure 8, with $j_0 = 1$ and $j'_0 = -2$, and $\gamma_1 = 1$ and $\gamma_2 = 3$.

A similar result is obtained when one considers as initial distribution of currents that corresponding to the antisymmetric dynamics of Figure 9.

6.2 Blow-up

At this point one may ask what happens when at $t = \tau$ the current is injected only at one of the 120 points. In order to address this question, we supposed that at time $t = \tau$ the only non-zero current is the one at point 1 of cell 5, that is, at the point labeled with 61. It is obvious that, due to the periodicity condition for which cell 1 is treated as adjacent to cell 10, the point of injection of the current could be the point 1 of any cell. We found that the solution blows up exponentially with time. In order to better appreciate such a behavior, in Figure 13 we report the solution for the case of 100 cells with the current injected only at point 601, that is, point 1 of cell 50.

One way to avoid this blow-up is to set $\gamma_1 = \gamma_2$, so there is no impedance mismatch, as done in the analysis of Lurie [17]. Then, if we start by injecting current at a single point, the field pattern degenerates to a single trajectory. The current flows either to the right or to the left in the space-time diagram: there are no reflected waves but only a transmitted wave. Conservation of current then implies that the current along the trajectory remains constant: there is no blow-up.

6.3 Eigenvalues and Eigenvectors of the Transfer Matrix

Now the question is: is it possible to obtain a solution that does not blow up without imposing any special constraint on the material parameters? To this purpose, let us calculate the eigenvalues of the transfer matrix. Clearly, with periodic boundary conditions, the transfer matrix is a $12M \times 12M$ matrix, and (6.2) gives its elements in terms of the Green function, whose components are explicitly given in Section 8. For simplicity, suppose we consider only 10 cells, for a total of 120 points (12 points for each unit cell) so that the number of eigenvalues is equal to 120 (we write the transfer matrix as a 120×120 matrix that, applied to a vector with 120 components describing the current distribution in the 120 points at a certain time, provides the vector with 120 components representing the

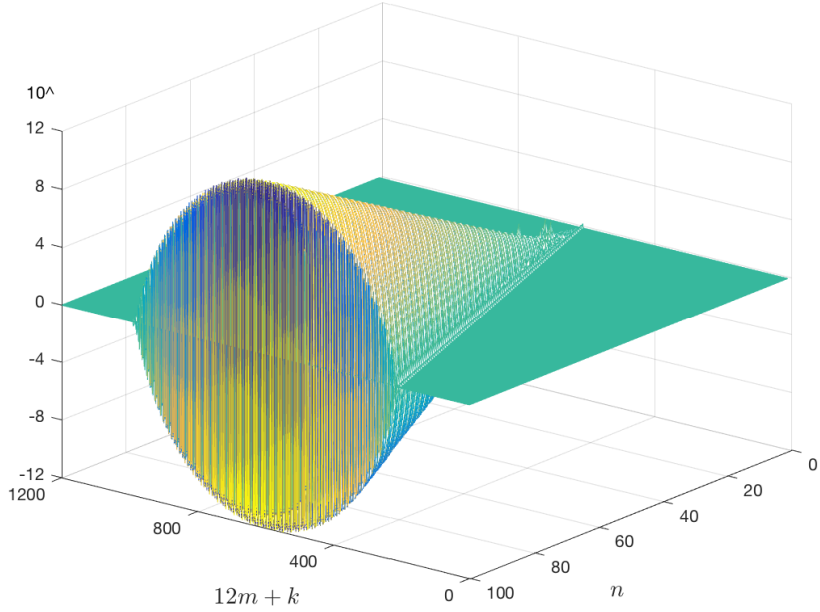


Figure 13: Evolution of the currents flow in 100 cells (1200 points in total), for $t = \tau + nt_0$ with $n = 0, 1, \dots, 100$, in the case when a unitary current is injected only at point 1 of cell 50, that is, at the point labeled with 601. The solution, here represented in logarithmic scale, blows up exponentially.

currents in the same 120 points after a period of time). For the particular case when $\gamma_1 = 1$ and $\gamma_2 = 3$, these eigenvalues are plotted in Figure 14. From the graph it is clear that many eigenvalues are on the unit circle. This is a consequence of the \mathcal{PT} symmetry of the system. Here \mathcal{P} stands for parity symmetry, the reflection invariance of the microstructure under spatial reflection $x \rightarrow -x$ when the origin is chosen at the center of an inclusion, and \mathcal{T} stands for time symmetry, the reflection invariance of the microstructure under time reversal $t \rightarrow -t$ (when again the origin is chosen at the center of an inclusion). Excellent reviews of \mathcal{PT} symmetry and its application to optics are given by Suchkov, Sukhorukov, Huang, Dmitriev, Lee, and Kivshar [62] and Konotop, Yang and Zezyulin [63]. It may seem that the time reversal symmetry is broken in our discrete dynamics, by the choice of τ . Note, however, that nothing really changes if we modify τ so long as the line $t = \tau$ does not intersect the inclusions: one just has to label the currents appropriately so they are consistent at the different values of τ . Thus if the line $t = \tau$ moves through a point where two current lines cross, then the ordering of the current numbering labels undergoes a swap. One can even choose τ so the line $t = \tau$ is exactly midway between two rows of inclusions, and then one clearly has time reversal symmetry. Nothing really changes, but at the points of intersection of two current lines one has to be careful to distinguish the current flowing upwards to the right from the current flowing upwards to the left.

Clearly modes having eigenvalues with modulus greater than 1 blow up in time, those with eigenvalues having modulus less than 1 decay in time, while those with eigenvalue having modulus 1 oscillate with time. Among all the eigenvalues, we select those with modulus equal to 1, and we apply the corresponding eigenvector as the initial current distribution in each unit cell. If $\gamma_1 = 1$ and $\gamma_2 = 3$ there are 99 eigenvalues with modulus 1 in total: the real one has multiplicity 3, whereas among the 96 complex eigenvalues the independent ones sum up to 13 pairs (each pair includes one eigenvalue together with its complex conjugate). In particular, 7 couples have negative real part and 6 positive real part. The results can be grouped into 3 classes: solutions periodic both in time and space with time period equal to t_0 and space period equal to $2x_0$, solutions periodic both in time and space but with period larger than t_0 and $2x_0$, and finally, solutions that are not periodic. To the first class belong the symmetric (Figure 8) and antisymmetric (Figure 9) dynamics considered in the two previous subsection and, therefore, we refer to Figure 12. Solutions of the second type are shown, as an example, in Figure 15, whereas solutions of the third type are given, for instance, in Figures 16 and 17.

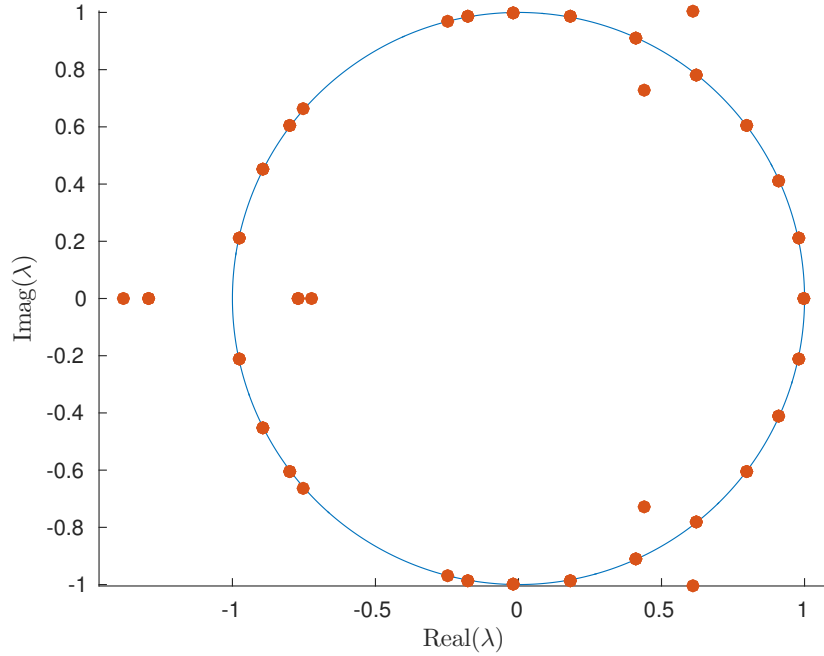


Figure 14: Eigenvalues of the transfer matrix in the case $\gamma_1 = 1$ and $\gamma_2 = 3$.

7 Conclusions

This paper launches the study of field patterns, but leaves many avenues for further research. In particular, it should motivate subsequent investigations on how things change if there is a small non-linearity (of possible relevance to quantum mechanics); how things change if the tensor $\sigma(\mathbf{x})$ has a small imaginary part (of possible relevance to determining the effective behavior of composites of hyperbolic metamaterials, when $\sigma(\mathbf{x})$ is replaced by the dielectric tensor field $\varepsilon(\mathbf{x})$ and time is replaced by a spatial variable); how things change if one considers the wave equation in two or three spatial dimensions, rather than just one; how things change if one looks at field patterns associated with other equations such as Maxwell's equations with a space time microstructure, or perhaps a modified version of Dirac's equation that allows one to insert some space time microstructure. A key point is that the underlying wave equation, in the ideal case, should not have any dispersion since otherwise the field patterns will lose their structure. Also our analysis begs the question as to whether there are space-time microstructures that give rise to field patterns, with appropriate moduli such that the transfer matrix only has eigenvalues with modulus 1, so that there are no growing modes. Additionally, from the viewpoint of homogenization, and high frequency homogenization [1, 64, 65, 66, 67, 68, 69, 70] in particular, one would like to know if there are solutions that have rapid oscillations at the scale of the cells, but which have macroscopic modulations and one would want to describe the effective equations that describe how these modulations propagate. It will be exciting to see how our understanding develops.

Acknowledgements

The authors are grateful to the Minneapolis Institute for Mathematics and its Applications for support as part of the special year on Mathematics and Optics. They also thank the National Science Foundation for support through grant DMS-1211359. Alexander and Natasha Movchan, and Hoai-Minh Nguyen are thanked for comments on the manuscript. Maxence Cassier is thanked for suggesting that we plot the eigenvalues of the transfer matrix. Carme Calderer is thanked for interesting discussions about liquid crystals with space-time microstructures.

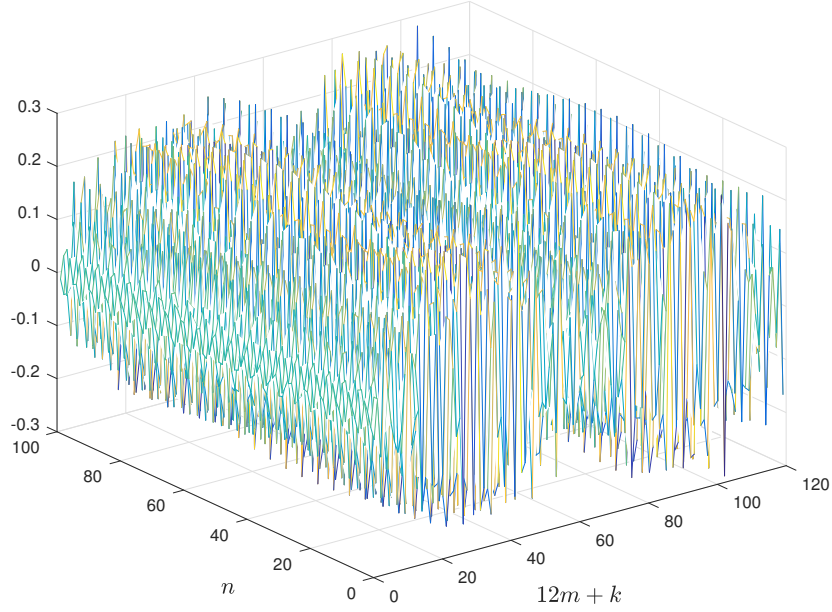


Figure 15: Evolution of the currents flow in 100 cells for $t = \tau + nt_0$ with $n = 0, 1, \dots, 100$, in the case when $\gamma_1 = 1$ and $\gamma_2 = 3$ and, at $t = \tau$ ($n=0$), we inject a distribution of currents equal to that given by the sum of one of the couples of two conjugate eigenvectors corresponding to the eigenvalues $-0.9775 \pm 0.211i$ (with multiplicity 4). The current flows following a pattern that is periodic both in time and in space but the periodicity is not equal to that of the unit cell.

8 Appendix A: Green's function for the space-time microstructure with aligned geometry

In this section we give the components of the Green function associated with the space-time microstructure illustrated in Figure 3, where the rectangular inclusions are aligned. We inject unitary current at time $t = \tau$ at each of the 12 points marked by the 12 green dots on the line $t = \tau$ in Figure 7 and recall that at each time step currents injected into one cell, can generate currents at time $t = \tau + t_0$ not only in that cell, but also in the two neighboring cells. The Green function is calculated by determining how the currents split along the characteristics. Clearly, as the Green function only depends on $m - m'$, the case where the currents are injected at points in other cells is straightforward: one has just to suitably translate the expressions of the components of the Green function. Recall that $G_{k,k'}(m - m')$ gives the current at point k , with $k = 1, 2, \dots, 12$, of cell m , given the current at point k' , with $k' = 1, 2, \dots, 12$, of cell m' . Since this only depends on $m - m'$ [more precisely $(m - m') \bmod M$] it suffices to take $m' = 0$. Then $G_{k,k'}(m)$ gives the current at point k , with $k = 1, 2, \dots, 12$, of cell m , given the current at point k' , with $k' = 1, 2, \dots, 12$, of cell 0: $m = -1$ then refers to the cell on the left of cell 0, i.e. cell $M - 1$, and $m = +1$ refers to the cell on the right of

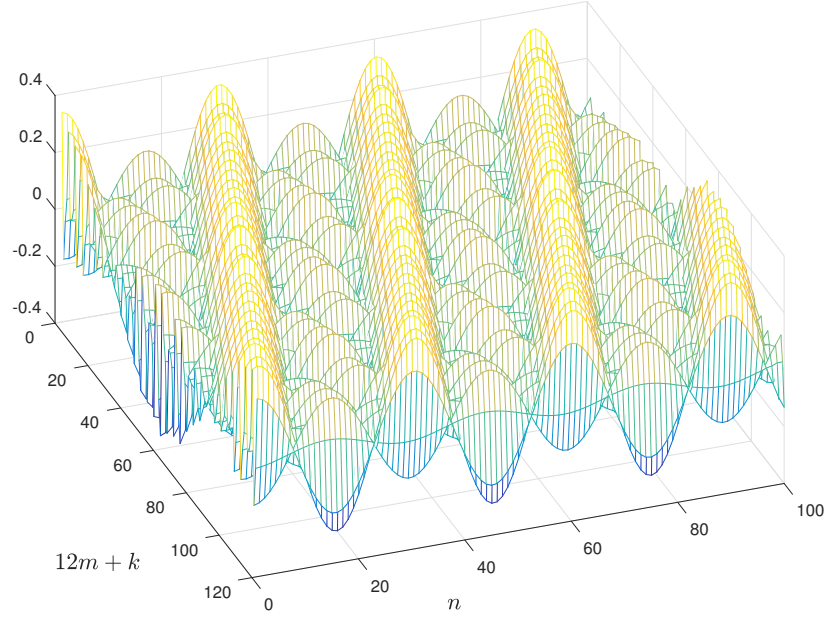


Figure 16: Evolution of the currents flow in 100 cells for $t = \tau + nt_0$ with $n = 0, 1, \dots, 100$, in the case when $\gamma_1 = 1$ and $\gamma_2 = 3$ and, at $t = \tau$ ($n=0$), we inject a distribution of currents equal to that given by the sum of one of the couples of two conjugate eigenvectors corresponding to the eigenvalues $0.9775 \pm 0.211i$ (with multiplicity 4). The current flows following a pattern that is not periodic.

cell 0, i.e. cell 1. So we see, step by step, if the current is injected at

$$\begin{aligned}
 \text{Point 1 of cell 0 : } j(1, 2, 0) = 1 & \Rightarrow \begin{cases} G(9, 1, -1) = 1; G(10, 1, -1) = \frac{\gamma_1 - \gamma_2}{\gamma_1 + \gamma_2}; \\ G(12, 1, -1) = -\frac{\gamma_1 - \gamma_2}{\gamma_1 + \gamma_2} \end{cases} \\
 \text{Point 2 of cell 0 : } j(2, 2, 0) = 1 & \Rightarrow G(1, 2, 0) = -\frac{\gamma_1 - \gamma_2}{\gamma_1 + \gamma_2}; G(3, 2, 0) = \frac{\gamma_1 - \gamma_2}{\gamma_1 + \gamma_2}; G(6, 2, 0) = 1 \\
 \text{Point 3 of cell 0 : } j(3, 2, 0) = 1 & \Rightarrow G(11, 3, -1) = 1 \\
 \text{Point 4 of cell 0 : } j(4, 2, 0) = 1 & \Rightarrow G(8, 4, 0) = 1 \\
 \text{Point 5 of cell 0 : } j(5, 2, 0) = 1 & \Rightarrow G(1, 5, 0) = 1; G(4, 5, 0) = \frac{\gamma_1 - \gamma_2}{\gamma_1 + \gamma_2}; G(6, 5, 0) = -\frac{\gamma_1 - \gamma_2}{\gamma_1 + \gamma_2} \\
 \text{Point 6 of cell 0 : } j(6, 2, 0) = 1 & \Rightarrow G(7, 6, 0) = -\frac{\gamma_1 - \gamma_2}{\gamma_1 + \gamma_2}; G(9, 6, 0) = \frac{\gamma_1 - \gamma_2}{\gamma_1 + \gamma_2}; G(10, 6, 0) = 1 \\
 \text{Point 7 of cell 0 : } j(7, 2, 0) = 1 & \Rightarrow G(3, 7, 0) = 1; G(4, 7, 0) = \frac{\gamma_1 - \gamma_2}{\gamma_1 + \gamma_2}; G(6, 7, 0) = -\frac{\gamma_1 - \gamma_2}{\gamma_1 + \gamma_2} \\
 \text{Point 8 of cell 0 : } j(8, 2, 0) = 1 & \Rightarrow G(7, 8, 0) = -\frac{\gamma_1 - \gamma_2}{\gamma_1 + \gamma_2}; G(9, 8, 0) = \frac{\gamma_1 - \gamma_2}{\gamma_1 + \gamma_2}; G(12, 8, 0) = 1 \\
 \text{Point 9 of cell 0 : } j(9, 2, 0) = 1 & \Rightarrow G(5, 9, 0) = 1 \\
 \text{Point 10 of cell 0 : } j(10, 2, 0) = 1 & \Rightarrow G(2, 10, 1) = 1 \\
 \text{Point 11 of cell 0 : } j(11, 2, 0) = 1 & \Rightarrow \begin{cases} G(7, 11, 0) = 1; G(10, 11, 0) = \frac{\gamma_1 - \gamma_2}{\gamma_1 + \gamma_2}; \\ G(12, 11, 0) = -\frac{\gamma_1 - \gamma_2}{\gamma_1 + \gamma_2} \end{cases} \\
 \text{Point 12 of cell 0 : } j(12, 2, 0) = 1 & \Rightarrow \begin{cases} G(1, 12, 1) = -\frac{\gamma_1 - \gamma_2}{\gamma_1 + \gamma_2}; G(3, 12, 1) = \frac{\gamma_1 - \gamma_2}{\gamma_1 + \gamma_2}; \\ G(4, 12, 1) = 1 \end{cases}
 \end{aligned}$$

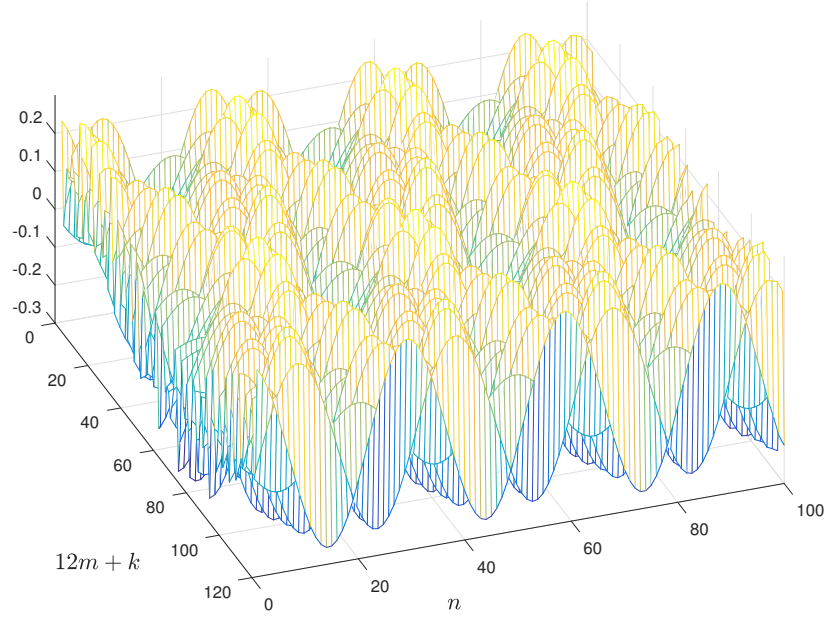


Figure 17: Evolution of the currents flow in 100 cells for $t = \tau + nt_0$ with $n = 0, 1, \dots, 100$, in the case when $\gamma_1 = 1$ and $\gamma_2 = 3$ and, at $t = \tau$ ($n=0$), we inject a distribution of currents equal to that given by the sum of one of the couples of two conjugate eigenvectors corresponding to the eigenvalues $0.9775 \pm 0.211i$ (with multiplicity 4). The current flows following a pattern that is not periodic.

Obviously, all the other components are equal to zero.

9 Appendix B: Solving the cell problem for a space-time microgeometry with staggered inclusions

In this Section we aim at deriving moduli that could partially govern the effective behavior of the dynamic composite material having the staggered inclusion microstructure shown in Figure 4 of the main text. We use the same procedure used for the space-time geometry with aligned inclusions, illustrated in Figure 3 of the main text and presented in Section 3 of the main text. In particular, we consider the same initial conditions applied in Section 3 of the main text so that the potentials $V_i^+(x, t)$ and $V_i^-(x, t)$ and the corresponding currents are still described by equations (3.2) and (3.3), respectively.

Note that the only difference between the microstructure with aligned inclusions (Figure 3 in the main text) and that with staggered inclusions (Figure 4 in the main text) consists in the fact that for the latter the unit cell of the dynamics network has the same dimensions of the unit cell of the geometry, that is x_0 and t_0 . This also implies that the unit cell has no symmetries and, therefore, we cannot separate the behavior into symmetric and antisymmetric dynamics. However, we can still look for distributions of currents such that the only non-zero component of the average current (and average electric field) is either in the time direction or in the space direction as shown here in Figure 19 and Figure 20, respectively. The unit cell can be taken to be that outlined by the dashed magenta lines in Figure 18.

Let us start by considering the dynamics depicted here in Figure 19: all the currents are flowing in the direction of positive time, and have the magnitudes $j_0, j_1, j_2, j_3, j_4, j_5$, and j_6 as indicated on the lines in Figure 19. Periodicity ensures the current flow has this structure. By conservation of current at the interfaces between the phases, we require that

$$j_1 + j_2 = j_5 + j_6. \quad (9.1)$$

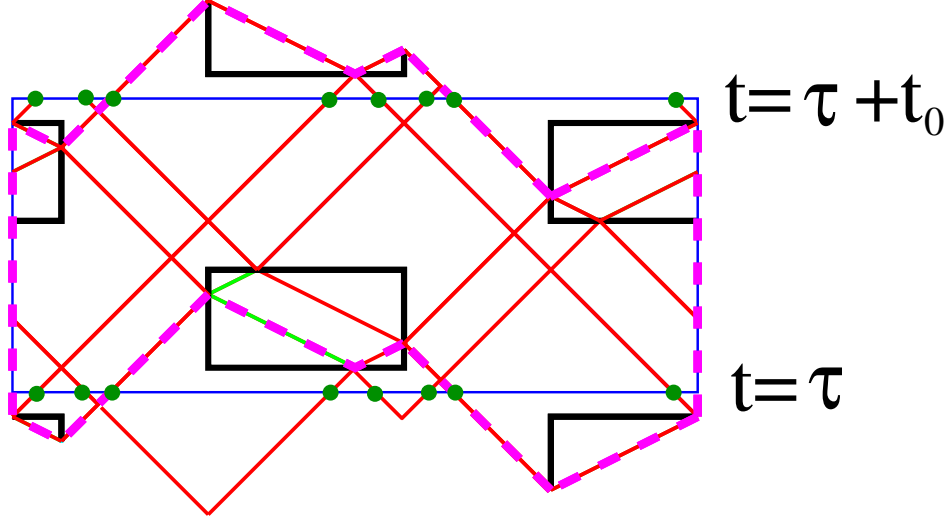


Figure 18: Outlined by the purple dashed lines is the unit cell of periodicity for the staggered cell dynamics of the microgeometry shown in Figure 4 of the main text in the case of a periodic field pattern. The red lines denote characteristic lines. The current flows along such lines and, across them, there is a jump in potential. Note that the dynamics splits into dynamics that are symmetric and antisymmetric with respect to reflection about the vertical centerline of the cell. We call these the symmetric dynamics and the antisymmetric dynamics. If the field pattern is not periodic then we can still consider a periodic array of the characteristic lines, and the period cell could be taken to be that outlined in blue. Current injected at time $t = \tau$ at any of the 8 points marked by the green dots at the bottom of the unit cell can contribute towards the excitation of the same field pattern. This current exits the unit cell at time $t = \tau + t_0$ at any of the 8 points marked by the green dots at the top of the unit cell, and may flow to the exit points of adjoining unit cells as well.

With reference to Figure 19 here, we let V_i , $i = 1, 2, \dots, 12$ denote the potentials in each of the regions $1, 2, \dots, 12$ and we let V'_i , $i = 1, 3, 5, 6, \dots, 12$ denote the potentials in each of the regions $1', 3', 5', 6', \dots, 12'$. For simplicity, we set $V'_1 = 0$. Then, following the rule according to which the potential jump across a characteristic line is γ_i times the current flowing through it, we obtain

$$\begin{aligned}
V_2 &= \gamma_2 j_5, & V_3 &= \gamma_2(j_5 + j_6), & V'_3 &= 2\gamma_2 j_5, & V_4 &= V_6 = V'_6 = \gamma_2(j_5 + j_6) + \gamma_1 j_1 = 2\gamma_2 j_5 + \gamma_1 j_2, \\
V_5 &= 2\gamma_2 j_5 + \gamma_1(j_1 + j_2), & V'_5 &= 2\gamma_2 j_5 + 2\gamma_1 j_2, & V_7 &= 2\gamma_2 j_5 + \gamma_1(j_2 - j_3), \\
V_8 &= \gamma_2(2j_5 + j_6) + \gamma_1(j_2 - j_3), & V'_8 &= 3\gamma_2 j_5 + \gamma_1(j_2 - j_4), & V_9 &= \gamma_2(j_5 + j_6) + \gamma_1(j_2 - j_3), \\
V_{10} &= V_{11} = \gamma_2(j_5 + j_6) - \gamma_1 j_3, & V'_{10} &= V'_{11} = 2\gamma_2 j_5 - \gamma_1 j_4 = \gamma_1 j_4, & V'_7 &= 2\gamma_2 j_5 + \gamma_1(j_2 - j_4), \\
V_{12} &= \gamma_2(j_5 + j_6) - \gamma_1(j_1 + j_3), & V'_{12} &= \gamma_1(j_4 - j_2).
\end{aligned} \tag{9.2}$$

Thus, in addition to (9.1), we have two further constraints:

$$\gamma_2(j_6 - j_5) = \gamma_1(j_2 - j_1), \quad \gamma_2 j_5 = \gamma_1 j_4. \tag{9.3}$$

A fourth relation can be obtained by imposing $V_1 = 0$ and by evaluating the potential V_{10} clockwise (as $V_{10} = 2\gamma_2 j_6 - \gamma_1 j_3$) and then anticlockwise ($V_{10} = \gamma_2 j_3$), to give

$$\gamma_2 j_6 = \gamma_1 j_3 \tag{9.4}$$

So all the currents can be expressed in terms of only two independent currents, say j_1 and j_2 . Then,

$$\begin{aligned}
j_5 &= \frac{1}{2}(j_1 + j_2) - \frac{\gamma_1}{2\gamma_2}(j_2 - j_1), & j_4 &= \gamma_2 j_5 / \gamma_1, \\
j_6 &= \frac{1}{2}(j_1 + j_2) + \frac{\gamma_1}{2\gamma_2}(j_2 - j_1), & j_3 &= \gamma_2 j_6 / \gamma_1.
\end{aligned} \tag{9.5}$$

As already pointed out, the current distribution shown in Figure 19 is such that the average current field is only in the time direction and it is easily worked out from the flux of current into the lower boundary of the cell of Figure 19: $(2j_1 + 2j_2 + j_3 + j_4 + 2j_5 + 2j_6)/x_0$. The average electric field can be easily determined from the potential jump across the cell in the vertical direction, and is $(V'_1 - V'_5)/t_0$. The ratio of the average current field divided by the average electric field is then given by

$$\frac{(2j_1 + 2j_2 + j_3 + j_4 + 2j_5 + 2j_6)/x_0}{(V'_1 - V'_5)/t_0} = -\frac{t_0(2j_1 + 2j_2 + j_3 + j_4 + 2j_5 + 2j_6)}{2x_0(\gamma_1 j_2 + \gamma_2 j_5)} = -\frac{t_0(4\gamma_1 + \gamma_2)}{x_0\gamma_1(\gamma_1 + \gamma_2)} \quad (9.6)$$

and this corresponds to the effective conductivity coefficient in the time direction $-\beta_*$.

To derive the effective conductivity coefficient in the space direction, α_* , we consider the current distribution illustrated here in Figure 20, where, as before, we assign the convention that currents flowing in the direction of positive time have positive sign, and currents flowing in the direction of negative time have negative sign. The currents are still labelled j_1, j_2, j_3, j_4, j_5 , and j_6 on the lines in Figure 20. Periodicity ensures the current flow has this structure. By conservation of current at the interfaces between the phases, we require that

$$j_1 + j_2 = j_5 + j_6, \quad j_3 = -j_6, \quad j_4 = -j_5. \quad (9.7)$$

We let $V_i, i = 1, 2, \dots, 12$ denote the potentials in each of the regions $1, 2, \dots, 12$ and we let $V'_i, i = 1, 3, 5, 6, \dots, 12$ denote the potentials in each of the regions $1, 3, 5, 6, \dots, 12$. Once again, for simplicity, we set $V'_1 = 0$. Then, from the rule that the potential jump across a characteristic line is γ_i times the current flowing through it, we have

$$\begin{aligned} V_2 &= \gamma_2 j_5, & V_3 &= V_5 = \gamma_2(j_5 - j_6), & V'_3 &= V'_5 = 0, & V_4 &= -\gamma_1 j_1 + \gamma_2(j_5 - j_6) = -\gamma_1 j_2, \\ V_6 &= \gamma_1 j_1 + \gamma_2(j_5 - j_6), & V'_6 &= \gamma_1 j_2, & V_7 &= \gamma_1(j_1 + j_3) + \gamma_2(j_5 - j_6), & V'_7 &= \gamma_1(j_2 + j_4), \\ V_8 &= \gamma_1(j_1 + j_3) + \gamma_2(j_5 - 2j_6), & V'_8 &= \gamma_1(j_2 + j_4) - \gamma_2 j_5, & V_9 &= \gamma_1(j_1 + j_3) + 2\gamma_2(j_5 - j_6), \\ V_{10} &= \gamma_1 j_3 + \gamma_2(j_5 - j_6), & V'_{10} &= \gamma_1 j_4, & V_{11} &= \gamma_1(2j_1 + j_3) + \gamma_2(j_5 - j_6), \\ V'_{11} &= \gamma_1(2j_2 + j_4), & V_{12} &= \gamma_1(j_1 + j_3) + \gamma_2(j_5 - j_6), & V'_{12} &= \gamma_1(j_2 + j_4). \end{aligned} \quad (9.8)$$

So in addition to (9.7) the currents must satisfy the constraint

$$\gamma_1(j_1 - j_2) = \gamma_2(j_5 - j_6). \quad (9.9)$$

Therefore, we can choose j_1 , and j_2 independently, and in terms of these

$$\begin{aligned} j_4 = -j_5 &= -\frac{1}{2}(j_1 + j_2) + \frac{\gamma_1}{2\gamma_2}(j_2 - j_1), \\ j_3 = -j_6 &= -\frac{1}{2}(j_1 + j_2) - \frac{\gamma_1}{2\gamma_2}(j_2 - j_1). \end{aligned} \quad (9.10)$$

As $V'_5 = V'_1$ there is no average electric field in the vertical direction. Similarly, there is no current field in the vertical direction. In the horizontal direction, by looking at the current flux out of the unit cell, one sees the average current to the right is $(j_2 + j_6 - j_1 - j_5)/t_0$. The average electric field pointing to the right is $(V'_{11} - V_{11})/x_0$. The ratio of the average current field divided by the average electric field is then

$$\frac{(j_2 + j_6 - j_1 - j_5)/t_0}{(V'_{11} - V_{11})/x_0} = \frac{x_0(\gamma_1 + \gamma_2)}{t_0\gamma_1(3\gamma_2 + \gamma_1)}, \quad (9.11)$$

and this corresponds to the effective conductivity coefficient in the space direction, α_* .

Therefore, the "effective conductivity tensor" for the staggered dynamics array is given by

$$\sigma_* = \begin{pmatrix} \alpha_* & 0 \\ 0 & -\beta_* \end{pmatrix} = \begin{pmatrix} \frac{x_0(\gamma_1 + \gamma_2)}{t_0\gamma_1(\gamma_1 + 3\gamma_2)} & 0 \\ 0 & -\frac{t_0(4\gamma_1 + \gamma_2)}{x_0\gamma_1(\gamma_1 + \gamma_2)} \end{pmatrix} = \begin{pmatrix} \frac{c_1(c_1 + 3c_2)(\gamma_1 + \gamma_2)}{\gamma_1(c_1 + c_2)(3\gamma_2 + \gamma_1)} & 0 \\ 0 & -\frac{(c_1 + c_2)(4\gamma_1 + \gamma_2)}{\gamma_1 c_1(c_1 + 3c_2)(\gamma_1 + \gamma_2)} \end{pmatrix}. \quad (9.12)$$

Then, the associated "effective speed of propagation" of the waves is

$$c_* = \sqrt{\alpha_*/\beta_*} = \frac{c_1(c_1 + 3c_2)(\gamma_1 + \gamma_2)}{(c_1 + c_2)\sqrt{(3\gamma_2 + \gamma_1)(4\gamma_1 + \gamma_2)}}. \quad (9.13)$$

Once again, this does not approach the wave velocity c_1 , even when the parameters of phase 2 approach those of phase 1. If we had chosen our units of space and time so that $x_0 = 1$ and $t_0 = 1$ then the corresponding dimensionless speed would be

$$\frac{c_* t_0}{x_0} = \frac{\gamma_1 + \gamma_2}{\sqrt{(3\gamma_2 + \gamma_1)(4\gamma_1 + \gamma_2)}}. \quad (9.14)$$

Again, we emphasize that we have put quotes around "effective conductivity tensor" and "effective speed" because at this stage it is unclear what is their physical significance. As remarked in the main text, if the conductivity tensor field $\sigma(\mathbf{x})$ had a very tiny imaginary part (as relevant to composites of hyperbolic materials, when $\sigma(\mathbf{x})$ is replaced by the dielectric tensor field $\epsilon(\mathbf{x})$, and time is replaced by a spatial variable) then indeed σ_* would be the appropriate "speed" giving the effective "characteristic lines" of propagation. In the absence of such an imaginary part one needs to derive the appropriate homogenized equations. This homogenized equation is unlikely to be simply $\nabla \cdot \sigma_* \nabla \underline{V} = 0$ where $\underline{V}(\mathbf{x})$ is some coarse grained potential, as it is quite evident from the branching nature of field patterns that there should be some term giving dispersion in the effective equations.

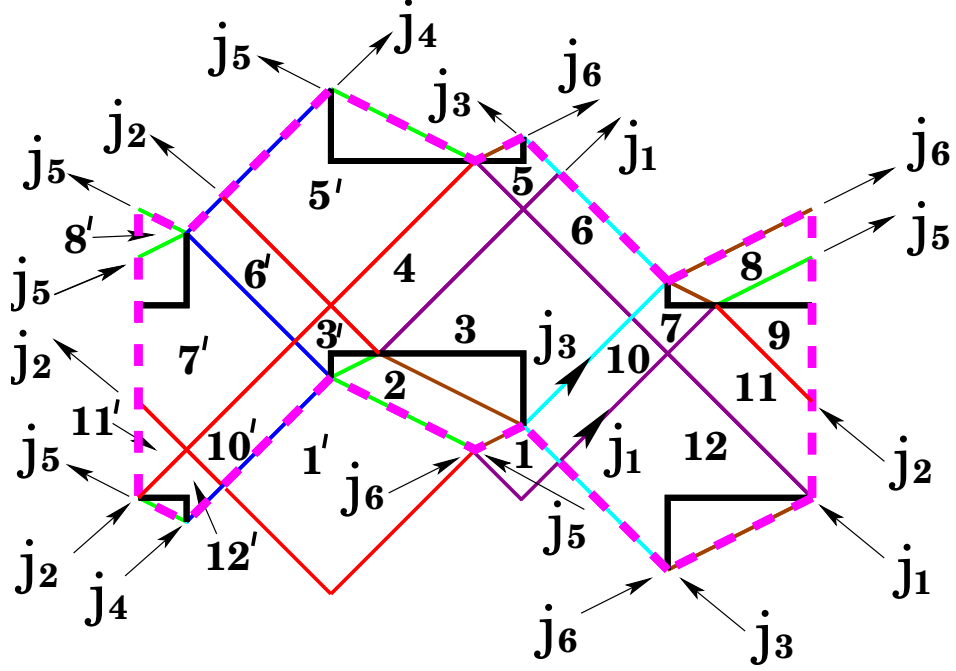


Figure 19: The current flows in the unit cell for the staggered array dynamics with the average electric and current fields directed along the time axis.

We tested the theoretical results obtained here by using the same procedure adopted for the aligned dynamics array in Section 5 of the main text. In particular, by choosing as test points the points of intersection between the characteristics and the horizontal line $t = \tau$, as in Figure 18, we obtain 8 test points. As before, we calculate, as detailed below, the Green function that allows one to determine the transfer matrix that gives the distribution of currents at a certain time $t = \tau + n t_0$ with n fixed, given the currents at time $t = \tau + (n - 1) t_0$.

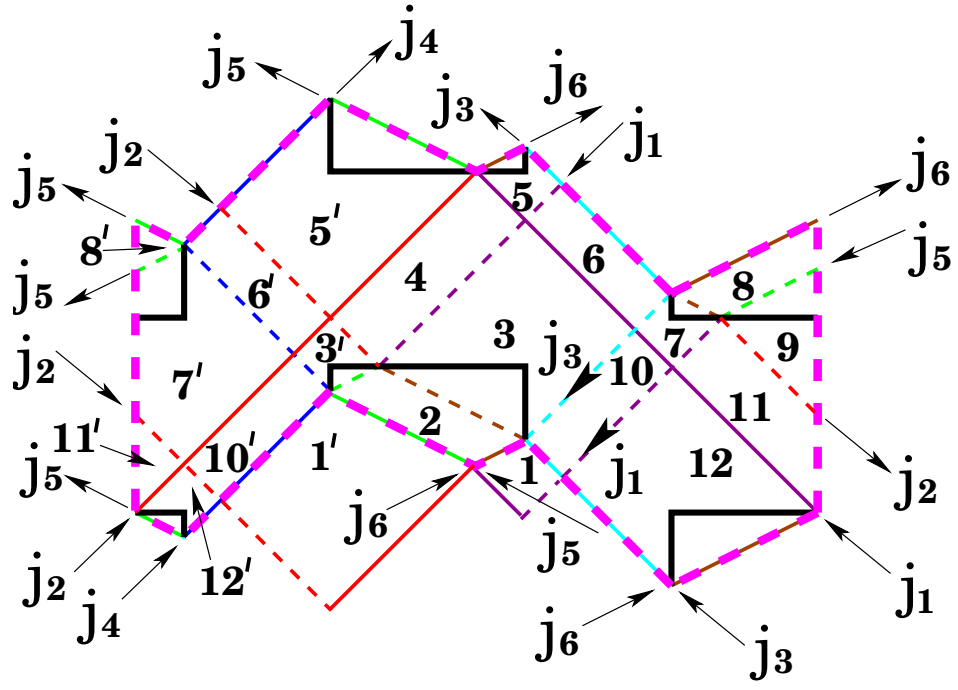


Figure 20: The current flows in the unit cell for the staggered array dynamics with the average electric and current fields directed along the space axis. Here the dashed lines denote currents in the negative time direction, i.e. a current j_1 flowing in the negative time direction is equivalent to a current $-j_1$ flowing in the positive time direction.

10 Appendix C: Green's function for the space-time staggered inclusion microstructure

By using the notation introduced in Section 6 of the main text, the components of the Green function related to the staggered geometry are given step by step by injecting current at the following points:

$$\begin{aligned}
\text{Point 1 of cell 0 : } j(1, 2, 0) = 1 & \Rightarrow G(4, 1, 0) = 1 \\
\text{Point 2 of cell 0 : } j(2, 2, 0) = 1 & \Rightarrow G(7, 2, -1) = 1; G(1, 2, 0) = \frac{\gamma_1 - \gamma_2}{\gamma_1 + \gamma_2}; G(3, 2, 0) = -\frac{\gamma_1 - \gamma_2}{\gamma_1 + \gamma_2} \\
\text{Point 3 of cell 0 : } j(3, 2, 0) = 1 & \Rightarrow \begin{cases} G(8, 3, -1) = -\frac{\gamma_1 - \gamma_2}{\gamma_1 + \gamma_2}; G(1, 3, 0) = -\frac{(\gamma_1 - \gamma_2)^2}{(\gamma_1 + \gamma_2)^2}; \\ G(2, 3, 0) = \frac{\gamma_1 - \gamma_2}{\gamma_1 + \gamma_2}; G(3, 3, 0) = \frac{(\gamma_1 - \gamma_2)^2}{(\gamma_1 + \gamma_2)^2}; G(6, 3, 0) = 1 \end{cases} \\
\text{Point 4 of cell 0 : } j(4, 2, 0) = 1 & \Rightarrow \begin{cases} G(8, 4, -1) = -\frac{\gamma_1 - \gamma_2}{\gamma_1 + \gamma_2}; G(1, 4, 0) = -\frac{(\gamma_1 - \gamma_2)^2}{(\gamma_1 + \gamma_2)^2}; \\ G(2, 4, 0) = \frac{\gamma_1 - \gamma_2}{\gamma_1 + \gamma_2}; G(3, 4, 0) = \frac{(\gamma_1 - \gamma_2)^2}{(\gamma_1 + \gamma_2)^2}; \\ G(7, 4, 0) = -\frac{\gamma_1 - \gamma_2}{\gamma_1 + \gamma_2}; G(8, 4, 0) = \frac{\gamma_1 - \gamma_2}{\gamma_1 + \gamma_2}; G(1, 4, 1) = 1 \end{cases} \\
\text{Point 5 of cell 0 : } j(5, 2, 0) = 1 & \Rightarrow \begin{cases} G(8, 5, -1) = 1; G(1, 5, 0) = \frac{\gamma_1 - \gamma_2}{\gamma_1 + \gamma_2}; G(3, 5, 0) = -\frac{\gamma_1 - \gamma_2}{\gamma_1 + \gamma_2}; \\ G(6, 5, 0) = \frac{\gamma_1 - \gamma_2}{\gamma_1 + \gamma_2}; G(7, 5, 0) = \frac{(\gamma_1 - \gamma_2)^2}{(\gamma_1 + \gamma_2)^2}; \\ G(8, 5, 0) = -\frac{(\gamma_1 - \gamma_2)^2}{(\gamma_1 + \gamma_2)^2}; G(1, 5, 1) = -\frac{\gamma_1 - \gamma_2}{\gamma_1 + \gamma_2} \end{cases} \\
\text{Point 6 of cell 0 : } j(6, 2, 0) = 1 & \Rightarrow G(7, 6, 0) = -\frac{\gamma_1 - \gamma_2}{\gamma_1 + \gamma_2}; G(8, 6, 0) = \frac{\gamma_1 - \gamma_2}{\gamma_1 + \gamma_2}; G(3, 6, 1) = 1 \\
\text{Point 7 of cell 0 : } j(7, 2, 0) = 1 & \Rightarrow \begin{cases} G(2, 7, 0) = 1; G(6, 7, 0) = \frac{\gamma_1 - \gamma_2}{\gamma_1 + \gamma_2}; G(7, 7, 0) = \frac{(\gamma_1 - \gamma_2)^2}{(\gamma_1 + \gamma_2)^2}; \\ G(8, 7, 0) = -\frac{(\gamma_1 - \gamma_2)^2}{(\gamma_1 + \gamma_2)^2}; G(1, 7, 1) = -\frac{\gamma_1 - \gamma_2}{\gamma_1 + \gamma_2} \end{cases} \\
\text{Point 8 of cell 0 : } j(8, 2, 0) = 1 & \Rightarrow G(5, 8, 0) = 1
\end{aligned}$$

Obviously, all the other components are equal to zero.

The eigenvalues of the transfer matrix, defined as $T_{(k,m),(k',m')} = G_{k,k'}(m - m')$, like in Section 6 of the main text, are plotted in Figure 21 in the case $\gamma_1 = 1$ and $\gamma_2 = 3$. Here we consider 10 cells, for a total of 80 points (8 points for each unit cell) so that the number of eigenvalues is equal to 80 (we write the transfer matrix as a 80×80 matrix that, applied to a vector with 80 components describing the current distribution at the 80 points at a certain time, provides the vector with 80 components representing the currents at the same 80 points after a cycle of time).

References

- [1] Bensoussan A, Lions JL, Papanicolaou GC. 1978 *Asymptotic Analysis for Periodic Structures*. Vol. 5 of Studies in Mathematics and its Applications. Amsterdam: North-Holland Publishing Co.
- [2] Attouch H. 1984 *Variational Convergence for Functions and Operators*. Applicable Mathematics Series. London: Pitman Publishing Ltd.
- [3] Zhikov VV, Kozlov SM, Oleinik OA. 1994 *Homogenization of Differential Operators and Integral Functionals*. Berlin / Heidelberg / London / etc.: Springer-Verlag. Translated from the Russian by G. A. Yosifian.

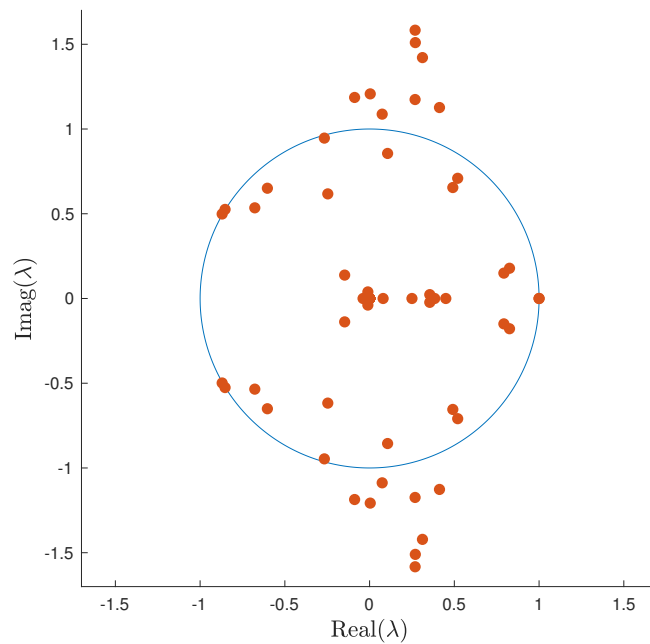


Figure 21: Eigenvalues of the transfer matrix in the case $\gamma_1 = 1$ and $\gamma_2 = 3$.

- [4] Tartar L. 2009 *The General Theory of Homogenization: a Personalized Introduction*. Vol. 7 of Lecture Notes of the Unione Matematica Italiana. Berlin / Heidelberg / London / etc.: Springer-Verlag.
- [5] Ngueseng G. 1989 A general convergence result for a functional related to the theory of homogenization. *SIAM J. Math. Anal.* **20**(3), 608–623.(doi:10.1137/0520043)
- [6] Allaire G. 1992 Homogenization and two-scale convergence. *SIAM J. Math. Anal.* **23**(6), 1482–1518. (doi:10.1137/0523084)
- [7] Couder Y, Protière S, Fort E, Boudaoud A. 2005 Dynamical phenomena: Walking and orbiting droplets. *Nature* **437**, 208. (doi:10.1038/437208a)
- [8] Couder Y, Fort E. 2006 Single-Particle Diffraction and Interference at a Macroscopic Scale. *Phys. Rev. Lett.* **97**(15), 154101. (doi:10.1103/PhysRevLett.97.154101)
- [9] Bush JWM. 2015 Pilot-wave hydrodynamics. *Ann. Rev. Fluid Mech.* **47**, 269–292. (doi:10.1146/annurev-fluid-010814-014506)
- [10] Lurie KA. 2007 *An Introduction to the Mathematical Theory of Dynamic Materials*. Vol. 15 of Advances in Mechanics and Mathematics. Berlin / Heidelberg / London / etc.: Springer-Verlag.
- [11] Louisell WH, Quate CF. 1958 Parametric Amplification of Space Charge Waves. *Proc. IRE.* **46**(4), 707–716. (doi:10.1109/JRPROC.1958.286771)
- [12] Cullen AL. 1958 A Travelling-Wave Parametric Amplifier. *Nature* **181**(4605), 332. (doi:10.1038/181332a0)
- [13] Tien PK. 1958 Parametric Amplification and Frequency Mixing in Propagating Circuits. *J. Appl. Phys.* **29**(9), 1347–1357. (doi:10.1063/1.1723440)
- [14] Morgenthaler FR. 1958 Velocity modulation of electromagnetic waves. *IRE Trans. Microw. Theory Techn.* **6**(2), 167–172. (doi:10.1109/TMTT.1958.1124533)

- [15] Fante RL. 1971 Transmission of electromagnetic waves into time-varying media. *IEEE Trans. Antennas Propag.* **19**(3), 417–424. (doi:10.1109/TAP.1971.1139931)
- [16] Honey RC, Jones EMT. 1960 A Wide-Band UHF Traveling-Wave Variable Reactance Amplifier. *IRE Trans.on Microw. Theory Techn.* **8**(3), 351–361. (doi: 10.1109/TMTT.1960.1125245)
- [17] Lurie KA. 1997 Effective properties of smart elastic laminates and the screening phenomenon. *Int. J. Solids Struc.* **34**(13), 1633–1643. (doi:10.1016/S0020-7683(96)00105-9)
- [18] Weekes SL. 2001 Numerical computation of wave propagation in dynamic materials. *Appl. Num. Math.* **37**(4), 417–440. (doi:10.1016/S0168-9274(00)00045-3)
- [19] Lurie KA, Weekes SL. 2003 Some new advances in the theory of dynamic materials. *J. Elast.* **72**(1), 229–239. (doi:10.1023/B:ELAS.0000018780.82718.19)
- [20] Lurie KA. 1998 The problem of effective parameters of a mixture of two isotropic dielectrics distributed in space-time and the conservation law for wave impedance in one-dimensional wave propagation. *Proc. R. Soc. A* **454**(1975), 1767–1779. (doi:10.1098/rspa.1998.0231)
- [21] To HT. 2009 Homogenization of dynamic laminates. *J. Math. Anal. Appl.* **354**(2), 518–538. (doi:10.1016/j.jmaa.2008.12.058)
- [22] Milton GW. 2002 *The Theory of Composites*. Vol. 6 of Cambridge Monographs on Applied and Computational Mathematics. Cambridge, UK: Cambridge University Press. Series editors: P. G. Ciarlet, A. Iserles, Robert V. Kohn, and M. H. Wright.
- [23] Cassedy ES, Oliner AA. 1963 Dispersion relations in time-space periodic media: Part I—Stable interactions. *Proc. IEEE* **51**(10), 1342–1359. (doi:10.1109/PROC.1963.2566)
- [24] Cassedy ES. 1965 Waves guided by a boundary with time-space periodic modulation. *Proc. IEEE* **112**(2), 269–279. (doi:10.1049/piee.1965.0040)
- [25] Chu RS, Tamir T. 1972 Wave propagation and dispersion in space-time periodic media. *Proc. IEEE* **119**(7), 797–806. (doi:10.1049/piee.1972.0169)
- [26] Cassedy ES. 1967 Dispersion relations in time-space periodic media: Part II—Unstable interactions. *Proc. IEEE* **55**(7), 1154–1168. (doi:10.1109/PROC.1967.5775)
- [27] Lurie KA, Weekes SL. 2006 Wave propagation and energy exchange in a spatio-temporal material composite with rectangular microstructure. *J. Math. Anal. Appl.* **314**(1), 286–310. (doi:10.1016/j.jmaa.2005.03.093)
- [28] Lurie KA, Onofrei D, Weekes SL. 2009 Mathematical analysis of the waves propagation through a rectangular material structure in space–time. *J. Math. Anal. Appl.* **355**(1), 180–194. (doi:10.1016/j.jmaa.2009.01.031)
- [29] Lurie KA, Yakovlev VV. 2016 Energy accumulation in waves propagating in space– and time–varying transmission lines. *IEEE Antennas Wireless Propag. Lett.* **15**, 1681–1684. (doi:10.1109/LAWP.2016.2522384)
- [30] Rousseau M, Maugin GA, Berezovski M. 2011 Elements of study on dynamic materials. *Arch. Appl. Mech.* **81**(7), 925–942. (doi:10.1007/s00419-010-0461-4)
- [31] Sanguinet WC. 2011 The homogenized equations of motion for an activated elastic lamination in plane strain. *ZAMM – J. Appl. Math. Mech.* **91**(12), 944–956. (doi:10.1002/zamm.201000208)
- [32] Maestre F, Münch A, Pedregal P. 2007 A spatio-temporal design problem for a damped wave equation. *J. Appl. Math.* **68**(1), 109–132. (doi:10.1137/07067965X)
- [33] Maestre F, Pedregal P. 2009 Dynamic materials for an optimal design problem under the two-dimensional wave equation. *Discrete Contin. Dyn. Syst. Ser. A* **23**(3), 973–990. (doi:10.3934/dcds.2009.23.973)
- [34] Jensen JS. 2009 Space-time topology optimization for one-dimensional wave propagation. *Comput. Method Appl. M.* **198**(5–8), 705–715. (doi:10.1016/j.cma.2008.10.008)

- [35] Jensen JS. 2010 Optimization of space-time material layout for 1D wave propagation with varying mass and stiffness parameter. *Control Cybern.* **39**(3), 599–614. (doi:doc/209716)
- [36] Yu Z, Fan S. 2009 Complete optical isolation created by indirect interband photonic transitions. *Nat. Photon.* **3**(1), 91–94. (doi:10.1038/nphoton.2008.273)
- [37] Lira H, Yu Z, Fan S, Lipson M. 2012 Electrically Driven Nonreciprocity Induced by Interband Photonic Transition on a Silicon Chip. *Phys. Rev. Lett.* **109**(3), 033901. (doi:10.1103/PhysRevLett.109.033901)
- [38] Taravati S, Caloz C. 2016 Mixer-Duplexer-Antenna Leaky-Wave System Based on Periodic Space-Time Modulation. *IEEE Trans. Antennas Propag.* **PP**(99), 1. (doi:10.1109/TAP.2016.2632735)
- [39] Fang K, Yu Z, Fan S. 2012 Realizing effective magnetic field for photons by controlling the phase of dynamic modulation. *Nat. Photon.* **6**, 782–787. (doi:10.1038/nphoton.2012.236)
- [40] Yuan L, Shi Y, Fan S. 2016 Photonic gauge potential in a system with a synthetic frequency dimension. *Opt. Lett.* **41**(4), 741–744. (doi:10.1364/OL.41.000741)
- [41] Boada O, Celi A, Latorre JI, Lewenstein M. 2012 Quantum Simulation of an Extra Dimension. *Phys. Rev. Lett.* **108**(13), 133001. (doi:10.1103/PhysRevLett.108.133001)
- [42] Celi A, Massignan P, Ruseckas J, Goldman N, Spielman IB, Juzeliunas G, et al. 2014 Synthetic Gauge Fields in Synthetic Dimensions. *Phys. Rev. Lett.* **112**(4), 173901. (doi:10.1103/PhysRevLett.112.043001)
- [43] Ozawa T, Price HM, Goldman N, Zilberberg O, Carusotto I. 2016 Synthetic dimensions in integrated photonics: From optical isolation to four-dimensional quantum Hall physics. *Phys. Rev. A* **93**(4), 043827. (doi:10.1103/PhysRevA.93.043827)
- [44] Zhang DW. 2016 Simulating Weyl points and nodal loops in an optical superlattice. *Quantum Inf. Proc.* **15**(11), 4477–4487. (doi:10.1007/s11128-016-1428-3)
- [45] Fisher RK, Gould RW. 1969 Resonance Cones in the Field Pattern of a Short Antenna in an Anisotropic Plasma. *Phys. Rev. Lett.* **22**(21), 1093–1095. (doi:10.1103/PhysRevLett.22.1093)
- [46] Naik GV, Shalaev VM, Boltasseva A. 2013 Alternative Plasmonic Materials: Beyond Gold and Silver. *Adv. Mater.* **25**(24), 3264–3294. (doi:10.1002/adma.201205076)
- [47] Korzeb K, Gajc M, Pawlak DA. 2015 Compendium of natural hyperbolic materials. *Opt. Express* **23**(20), 25406–25424. (doi:10.1364/OE.23.025406)
- [48] Jacob Z, Alekseyev LV, Narimanov E. 2006 Optical Hyperlens: Far-field imaging beyond the diffraction limit. *Opt. Express* **4**(18), 8247–8256. (doi:10.1364/OE.14.008247)
- [49] Salandrino A, Engheta N. 2006 Far-field subdiffraction optical microscopy using metamaterial crystals: Theory and simulations. *Phys. Rev. B* **74**(7), 075103. (doi:10.1103/PhysRevB.74.075103)
- [50] Rho J, Ye Z, Xiong Y, Yin X, Liu Z, Choi H, et al. 2010 Spherical hyperlens for two-dimensional sub-diffractive imaging at visible frequencies. *Nat. Commun.* **1**(9), 143. (doi:10.1038/ncomms1148)
- [51] Lu D, Liu Z. 2012 Hyperlenses and metalenses for far-field super-resolution imaging. *Nat. Commun.* **3**, 1205. (doi:10.1038/ncomms2176)
- [52] Krylov V, Sorokin SV. 1997 Dynamics of elastic beams with controlled distributed stiffness parameters. *Smart Mater. Struct.* **6**(5), 573–582. (doi:10.1088/0964-1726/6/5/008)
- [53] Sorokin SV, Ershova OA, Grishina SV. 2000 The active control of vibrations of composite beams by parametric stiffness modulation. *Eur. J. Mech. A-Solids* **19**(5), 873–890. (doi:10.1016/S0997-7538(00)00184-4)
- [54] Sorokin SV, Grishina SV. 2004 Analysis of wave propagation in sandwich beams with parametric stiffness modulations. *Jo. Sound Vib.* **271**(3–5), 1063–1082. (doi:10.1016/j.jsv.2003.03.003)

- [55] Fink M. 2016 From Loschmidt daemons to time-reversed waves. *Phil. Trans. R. Soc. A* **374**(2069), 20150156. (doi:10.1098/rsta.2015.0156)
- [56] Goussev A, Jalabert RA, Pastawski HM, Wisniacki DA. 2016 Theme issue ‘Loschmidt echo and time reversal in complex systems’. *Phil. Trans. R. Soc. A* **374**(2069), 20150156. (doi:10.1098/rsta.2015.0383)
- [57] Blekhman II. 2007 On vibratory dynamic materials and composites. *Doklady Phys.* **52**(6), 335–338. (doi:10.1134/S1028335807060110)
- [58] Movchan AB, Movchan NV, Milton GW. 2016 Field Patterns in Temporal Laminates. To be submitted.
- [59] Khruslov EY. 1978 The asymptotic behavior of solutions of the second boundary value problem under fragmentation of the boundary of the domain. *Matematicheskii Sbornik* **106**(4), 604–621. English translation in *Math. USSR Sb.* **35**, 266–282 (1979). (doi:10.1070/SM1979v035n02ABEH001474)
- [60] Briane M. 1998 Homogenization in some weakly connected domains. *Ricerche di Matematica (Napoli)* **47**(1), 51–94.
- [61] Briane M, Mazliak L. 1998 Homogenization of two randomly weakly connected materials. *Portugal. Math.* **55**(2), 187–207.
- [62] Suchkov SV, Sukhorukov AA, Huang J, Dmitriev SV, Lee C, Kivshar YS. 2016 Nonlinear switching and solitons in PT-symmetric photonic systems. *Laser Photon. Rev.* **10**(2), 177–213. (doi:10.1002/lpor.201500227)
- [63] Konotop VV, Yang J, Zezyulin DA. 2016 Nonlinear waves in \mathcal{PT} -symmetric systems. *Rev. Mod. Phys.* **88**(3), 035002. (doi/10.1103/RevModPhys.88.035002)
- [64] Birman MS, Suslina TA. 2006 Homogenization of a multidimensional periodic elliptic operator in a neighborhood of the edge of an internal gap. *J. Math. Sci.* **136**(2), 3682–3690. (doi:10.1007/s10958-006-0192-9)
- [65] Brassart M, Lenczner M. 2010 A two-scale model for the periodic homogenization of the wave equation. *J. Math. Pures Appl.* **93**(5), 474–517. (doi:10.1016/j.matpur.2010.01.002)
- [66] Craster RV, Kaplunov J, Pichugin AV. 2010 High frequency homogenization for periodic media. *Proc. R. Soc. A* **466**(2120), 2341–2362. (doi:10.1098/rspa.2009.0612)
- [67] Allaire G, Palombaro M, Rauch J. 2011 Diffractive geometric optics for Bloch waves. *Arch. Rat. Mech. Anal.* **202**(2), 373–426. (doi:10.1007/s00205-011-0452-9)
- [68] Hoefer MA, Weinstein MI. 2011 Defect Modes and Homogenization of Periodic Schrödinger Operators. *SIAM J. Math. Anal.* **43**(2), 971–996. (doi:10.1137/100807302)
- [69] Ceresoli L, Abdeddaim R, Antonakakis T, Maling B, Chmiao M, Sabouroux P, et al. 2015 Dynamic effective anisotropy: Asymptotics, simulations and microwave experiments with dielectric fibres. *Phys. Rev. B* **92**(17), 174307:1–174307:7. (doi:10.1103/PhysRevB.92.174307)
- [70] Harutyunyan D, Craster RV, Milton GW. 2016 High frequency homogenization for travelling waves in periodic media. *Proc. R. Soc. A* **472**(2191), 20160066. (doi:10.1098/rspa.2016.0066)